

DO-TH 2000/14

RBRC-148

TPR-00-21

hep-ph/0011215

October 2000

# Models for the Polarized Parton Distributions of the Nucleon

M. Glück<sup>a</sup>, E. Reya<sup>a</sup>, M. Stratmann<sup>b</sup>, W. Vogelsang<sup>c</sup>

<sup>a</sup>*Universität Dortmund, Institut für Physik,  
D-44221 Dortmund, Germany*

<sup>b</sup>*Institut für Theoretische Physik, Universität Regensburg  
D-93040 Regensburg, Germany*

<sup>c</sup>*RIKEN-BNL Research Center, Brookhaven National Laboratory  
Upton, NY 11973, USA*

## Abstract

Polarized deep inelastic scattering (DIS) data are analyzed in leading and next-to-leading order of QCD within the common ‘standard’ scenario of polarized parton distributions with a flavor-symmetric light sea (antiquark) distribution  $\delta\bar{q}$ , and a completely  $SU(3)_f$  broken ‘valence’ scenario with totally flavor-asymmetric light sea densities ( $\delta\bar{u} \neq \delta\bar{d} \neq \delta\bar{s}$ ). The latter flavor-broken light sea distributions are modelled with the help of a Pauli-blocking ansatz at the low radiative/dynamical input scales of  $\mu_{LO(NLO)}^2 = 0.26$  (0.40)  $\text{GeV}^2$  which complies with predictions of the chiral quark-soliton model and expectations based on the statistical parton model as well as with the corresponding, well established, flavor-broken unpolarized sea ( $\bar{d} > \bar{u}$ ). Present semi-inclusive DIS data cannot yet uniquely discriminate between those two flavor-symmetric and flavor-broken polarized light sea scenarios.

# 1 Introduction

The polarized parton distributions of the nucleon have been intensively studied in recent years [1 – 14]. The conclusion has been that the experimental data dictate a negatively polarized antiquark component, and show a tendency toward a positive polarization of gluons. Presently we possess a lot of precise data [15 – 24] on the polarized structure functions of the nucleon, some of them very recent [23, 24], which justify a renewed investigation of the aforementioned issue. This alone, however, does not provide the main motivation for this project, rather the improved understanding in recent years of the situation in the *unpolarized* parton sector [25 – 28] provides important insights for the corresponding *polarized* parton densities. In particular, one notes that the unpolarized sea (antiquark) distributions are flavor–asymmetric ( $\bar{d} > \bar{u}$ ), which can be understood in terms of flavor mass asymmetries and Pauli–blocking effects [29, 30]. The main objective of the present paper is to transcribe these insights into the polarized parton sector as will be described in Section 3. In Section 2 we shall, for completeness, present an analysis within the framework of the simplified  $SU(3)_f$  symmetric ‘standard’ scenario in which the flavor–asymmetries in the polarized antiquark sector are neglected. This is done in view of the fact that in many situations these flavor asymmetries are unobservable as is the case for (most) presently available data which cannot provide any reliable information concerning this issue.

Measurements of polarized deep–inelastic lepton nucleon scattering yield direct information [15 – 24] on the spin asymmetry

$$A_1^N(x, Q^2) \simeq \frac{g_1^N(x, Q^2)}{F_1^N(x, Q^2)} = \frac{g_1^N(x, Q^2)}{F_2^N(x, Q^2)/\{2x[1 + R^N(x, Q^2)]\}}, \quad (1.1)$$

$N = p, n$  and  $d = (p + n)/2$  where in the latter case we have used  $g_1^d = (g_1^p + g_1^n)[1 - 3\omega_D/2]/2$  with  $\omega_D = 0.058$ ,  $R \equiv F_L/2xF_1 = (F_2 - 2xF_1)/2xF_1$  and subdominant contributions have, as usual, been neglected.

We emphasize that, as in our original analysis [1], we compute *both*  $g_1$  and  $F_1$  entirely in leading-twist QCD. In particular, in order to obtain  $F_1$ , we use the parton densities of GRV98 [25] along with LO (note that  $R = 0$  at leading order) or NLO coefficient functions for  $F_2$  and  $R$  in (1.1). An alternative, frequently adopted [3, 4, 5, 9, 10, 13] approach is to take  $F_2(x, Q^2)$  and  $R(x, Q^2)$  from experimental measurements, which is motivated by the fact that leading-twist calculations of  $F_2(x, Q^2)$  and  $R(x, Q^2)$  do not agree very well with experimental determinations in the region of low  $Q^2$  and  $W^2 = Q^2(1-x)/x$ . These regions are affected by power-suppressed contributions and are therefore excluded from all unpolarized DIS analyses. The presently available data in the polarized case, however, do not allow to impose similarly ‘safe’ cuts ( $Q^2 \geq 4 \text{ GeV}^2$ ,  $W^2 \geq 10 \text{ GeV}^2$ ) without losing too much information. On the other hand, the  $Q^2$  range accessed so far in polarized DIS does not allow for extracting the magnitude and shape of power-suppressed contributions reliably. To study the issue further, we performed fits to the  $A_1$  data in both possible ways, i.e. with leading-twist calculations of  $F_2$  and  $R$  *as well as* with their experimental results, admitting at the same time an ‘effective higher-twist’ contribution to  $A_1$  in terms of a factor  $(1 + A(x)/Q^2)$  with  $A(x)$  to be determined by the data. The outcome of this analysis was that  $A(x)$  is consistent with zero if we use leading-twist QCD for  $F_2$  and  $R$ , but that it is sizeable and important in the fit if  $F_2$  and  $R$  are taken from experiment. We take this as an indication that our preferred approach is more consistent and less liable to modifications by higher-twist terms. This view is also corroborated by the fact that the DIS  $A_1$  data show only a very mild  $Q^2$ -dependence, even toward low values of  $Q^2$ . The consistency of the polarized parton densities as extracted from DIS data at comparatively low values of  $Q^2$  with measurements of other hard processes at higher scales can be studied soon at RHIC and perhaps in the future at a polarized  $ep$  collider.

In NLO,  $g_1^N(x, Q^2)$  is related to the polarized (anti)quark and gluon distributions

$\delta f(x, Q^2) \equiv f_+ - f_-$  in the following way:

$$g_1^N(x, Q^2) = \frac{1}{2} \sum_q e_q^2 \{ \delta q^N(x, Q^2) + \delta \bar{q}^N(x, Q^2) + \frac{\alpha_s(Q^2)}{2\pi} [\delta C_q * (\delta q^N + \delta \bar{q}^N) + \frac{1}{f} \delta C_g * \delta g] \} \quad (1.2)$$

with the convolutions  $\delta C_f * f$  being defined in the usual way. The  $\overline{\text{MS}}$  coefficient functions  $\delta C_f(x)$  can be also found in [1], where all necessary ingredients for the  $Q^2$ -evolution have been formulated as well. A similar expression holds for the unpolarized structure function  $F_1^N(x, Q^2)$  with its spin-averaged parton distributions  $f(x, Q^2) \equiv f_+ + f_-$  and the unpolarized Wilson coefficients can be found, for example, in [31]. The LO and NLO( $\overline{\text{MS}}$ ) input scales, running coupling constants and parton distributions, employed in the positivity constraints  $|\delta f| \leq f$ , will be adopted from GRV98 [25]. Furthermore we shall, as always, use the notation  $\delta q^p \equiv \delta q$  and  $q^p \equiv q$ , and neglect the marginal charm contribution to  $g_1^N$  stemming from the subprocess  $\bar{\gamma}^* \bar{g} \rightarrow c\bar{c}$  [32]. The charm contribution to  $F_1^N$  is also small in the kinematic range covered by present polarization experiments.

The total helicity of a specific parton  $f = u, \bar{u}, d, \bar{d}, s, \bar{s}, g$  is given by the first ( $n = 1$ ) moment

$$\Delta f(Q^2) \equiv \int_0^1 dx \delta f(x, Q^2). \quad (1.3)$$

Thus, according to (1.2),

$$\Gamma_1(Q^2) \equiv \int_0^1 dx g_1(x, Q^2) = \frac{1}{2} \sum_q e_q^2 [\Delta q(Q^2) + \Delta \bar{q}(Q^2)] \left( 1 - \frac{\alpha_s(Q^2)}{\pi} \right) \quad (1.4)$$

since  $\Delta C_q = -3C_F/2 = -2$  and  $\Delta C_g = 0$ . Therefore we have in general

$$\Gamma_1^{p,n}(Q^2) = \left[ \pm \frac{1}{12} \Delta q_3 + \frac{1}{36} \Delta q_8 + \frac{1}{9} \Delta \Sigma(Q^2) \right] \left( 1 - \frac{\alpha_s(Q^2)}{\pi} \right) \quad (1.5)$$

with the flavor-nonsinglet components

$$\Delta q_3 \equiv \Delta u + \Delta \bar{u} - \Delta d - \Delta \bar{d} \quad (1.6)$$

$$\Delta q_8 \equiv \Delta u + \Delta \bar{u} + \Delta d + \Delta \bar{d} - 2(\Delta s + \Delta \bar{s}) \quad (1.7)$$

being conserved, i.e.  $Q^2$ -independent, and the flavor-singlet component is given by

$$\Delta\Sigma(Q^2) \equiv \sum_{q=u,d,s} [\Delta q(Q^2) + \Delta\bar{q}(Q^2)] = \Delta q_8 + 3 [\Delta s(Q^2) + \Delta\bar{s}(Q^2)] . \quad (1.8)$$

These quantities will be subject to various constraints (derived from hyperon  $\beta$ -decays) depending on the specific model scenarios under consideration to which we shall turn in the next two Sections.

Finally, the fundamental helicity sum rule reads

$$\frac{1}{2} = \frac{1}{2}\Delta\Sigma(Q^2) + \Delta g(Q^2) + L_{q+g}(Q^2) \quad (1.9)$$

where  $L_{q+g}$  refers to the total orbital contribution of all (anti)quarks and gluons to the spin of the proton.

## 2 $SU(3)_f$ symmetric ‘standard’ (unbroken-sea) scenario

As stated in the Introduction, present data do not provide sufficient information concerning the flavor-asymmetries of the polarized sea distributions. Thus present day studies must, as a first approximation, neglect this issue unless one is willing to adopt some models for the flavor-asymmetries as will be done in Section 3. Here we follow the procedure presented in GRSV95 [1]. The searched for polarized NLO (as well as LO) parton distributions  $\delta f(x, Q^2)$ , compatible with present data [15 – 24] on  $A_1^N(x, Q^2)$ , are constrained by the ‘standard’ sum rules

$$\Delta q_3 = F + D = g_A = 1.2670 \quad (35) \quad (2.1)$$

$$\Delta q_8 = 3F - D = 0.58 \pm 0.15 \quad (2.2)$$

where the updated values for  $F$  and  $D$  have been taken into account [33] and the error estimate in Eq. (2.2) is due to [34]. Thus, Eq. (1.5) becomes

$$\Gamma_1^{p,n}(Q^2) = \left[ \pm \frac{1}{12}(F + D) + \frac{5}{36}(3F - D) + \frac{1}{3}(\Delta s(Q^2) + \Delta \bar{s}(Q^2)) \right] \left( 1 - \frac{\alpha_s(Q^2)}{\pi} \right), \quad (2.3)$$

i.e. one needs here a finite sizeable strange sea polarization  $\Delta s(Q^2) < 0$  in order to achieve the experimentally required reduction of the Ellis–Jaffe LO expectation [35]

$$\Gamma_{1,\text{EJ}}^p = \frac{1}{12}(F + D) + \frac{5}{36}(3F - D) \simeq 0.186. \quad (2.4)$$

Furthermore, in the ‘standard’ scenario one assumes an unbroken  $\text{SU}(3)_f$  symmetric sea,

$$\delta \bar{q}(x, Q^2) \equiv \delta \bar{u} = \delta u_{\text{sea}} = \delta \bar{d} = \delta d_{\text{sea}} = \delta s = \delta \bar{s}. \quad (2.5)$$

For the determination of the NLO (LO) polarized parton distributions  $\delta f(x, Q^2)$  we follow our original analysis [1] by relating the polarized input densities to the unpolarized ones, using some intuitive theoretical arguments [36] as guidelines. We employ the following ansatz for the LO and NLO( $\overline{\text{MS}}$ ) polarized parton distributions at an input scale  $Q^2 = \mu^2$  [37]:

$$\begin{aligned} \delta u(x, \mu^2) &= N_u x^{\alpha_u} (1-x)^{\beta_u} u(x, \mu^2)_{\text{GRV}} \\ \delta d(x, \mu^2) &= N_d x^{\alpha_d} (1-x)^{\beta_d} d(x, \mu^2)_{\text{GRV}} \\ \delta \bar{q}(x, \mu^2) &= N_{\bar{q}} x^{\alpha_{\bar{q}}} (1-x)^{\beta_{\bar{q}}} \bar{q}(x, \mu^2)_{\text{GRV}} \\ \delta g(x, \mu^2) &= N_g x^{\alpha_g} (1-x)^{\beta_g} g(x, \mu^2)_{\text{GRV}} \end{aligned} \quad (2.6)$$

with the LO and NLO unpolarized input densities referring to the ones of GRV98 [25] and  $\bar{q} \equiv (\bar{u} + \bar{d})/2$  should be considered as the reference light sea distribution for the ‘standard’ unbroken–sea scenario in (2.5). The parameters of our optimal LO densities at  $\mu_{\text{LO}}^2 = 0.26 \text{ GeV}^2$  and the ones of the NLO( $\overline{\text{MS}}$ ) densities at  $\mu_{\text{NLO}}^2 = 0.40 \text{ GeV}^2$  are given in Table I. These optimal LO and NLO( $\overline{\text{MS}}$ ) fits correspond to a  $\chi^2$  per degree of freedom ( $\chi_{\text{DF}}^2$ ) of  $\chi_{\text{DF,LO}}^2 = 0.84$  and to  $\chi_{\text{DF,NLO}}^2 = 0.81$ . The polarized gluon density in (2.6) is, as usual, rather weakly constrained by present data. Although a fully saturated (via

the positivity constraint) gluon input  $\delta g(x, \mu^2) = \pm g(x, \mu^2)$  is disfavored, a less saturated  $\delta g(x, \mu^2) = \pm xg(x, \mu^2)$  input or even a vanishing (purely dynamical) input  $\delta g(x, \mu^2) = 0$  are fully compatible with present data. The latter choice, however, seems to be unlikely in view of  $\delta \bar{q}(x, \mu^2) \neq 0$ .

In Fig. 1 our NLO results are compared with the data on  $A_1^N(x, Q^2)$  as well as with our old original NLO( $\overline{\text{MS}}$ ) fit [1]. The differences between these two results are small, except perhaps for  $A_1^p$  in the large- $x$  region. Our new LO fit is similar to the NLO one shown in Fig. 1 by the solid curves. The  $Q^2$ -dependence of our LO and NLO ‘standard’ scenario fits at various fixed values of  $x$  is shown in Fig. 2 and compared with all recent data on  $g_1^p(x, Q^2)$ , including the most recent E155 proton data [24]. The main reason for our LO results being larger than the NLO ones in the small- $x$  region is due to the vanishing of  $R^p(x, Q^2)$  in LO in (1.1). The corresponding  $x$ -dependence of  $g_1^N(x, Q^2 = 5 \text{ GeV}^2)$  is shown in NLO in Fig. 3 where the expected extrapolations into the yet unmeasured small- $x$  region down to  $x = 10^{-3}$  are shown as well. The solid curves refer to our optimal NLO fit (with the input given in Table I) and allowing our optimal total  $\chi^2$  in Table I to vary by one unit,  $\delta\chi^2 = \pm 1$ , gives rise to the shaded areas due to different choices of the polarized gluon input at  $Q^2 = \mu_{\text{NLO}}^2$  in (2.6) such as  $\delta g = \pm xg$ , etc. In particular a vanishing polarized gluon input  $\delta g(x, \mu_{\text{NLO}}^2) = 0$ , is for the time being entirely compatible with all present data as shown by the dashed curves. On the other hand, fully saturated (via the positivity constraint) gluon inputs  $\delta g(x, \mu_{\text{NLO}}^2) = \pm g$  appear to be disfavored by present data as shown by the dotted curves in Fig. 3. It should be furthermore noted that the shaded bands in Fig. 3 contain polarized gluon densities which correspond to first moments  $\Delta g(Q^2 = 5 \text{ GeV}^2)$  between  $-0.81$  and  $1.73$ , according to input moments between  $\Delta g(\mu_{\text{NLO}}^2) = -0.45$  and  $0.7$ , respectively, i.e. even negative total gluon polarizations are compatible with present data. The same results hold of course also in LO. Future dedicated polarized small- $x$  measurements and upcoming determinations of  $\delta g(x, Q^2)$  should be useful in removing such extrapolation ambiguities caused by our

present poor knowledge of  $\delta g(x, Q^2)$ .

Our corresponding LO and NLO parton distributions at the respective input scales  $Q^2 = \mu_{\text{LO, NLO}}^2$  in Eq. (2.6) with the ‘standard’ scenario fit parameters given in Table I are shown in Fig. 4. The main differences between our new input densities and our old GRSV95 ones [1] are somewhat harder  $\delta d$  (due to the new neutron data) and  $\delta g$  distributions although, as discussed above, the polarized gluon distribution in Fig. 4 is only slightly preferred by our ‘optimal’ fit to presently available data. The polarized input densities in Figs. 4(a) and 4(b) are compared with our reference unpolarized valence-like LO and NLO dynamical input densities of [25] which satisfy of course the positivity requirement  $|\delta f| \leq f$  as is obvious from Eq. (2.6). It should be nevertheless emphasized that the parameters, resulting from our rather general LO and NLO fits, are always such that these positivity conditions are automatically satisfied, i.e. there is practically no need to impose them separately. The distributions at  $Q^2 = 5 \text{ GeV}^2$ , as obtained from these LO and NLO inputs at  $Q^2 = \mu^2$ , are shown in Fig. 5 where they are also compared with our old NLO GRSV95 [1] results. It should be noted that the substantially harder input polarized gluon density  $x\delta g(x, \mu^2)$ , in particular in LO, in Fig. 4(a) as compared to our old GRSV95 fit, causes the sea density  $x\delta\bar{q}(x, Q^2)$  to oscillate (slightly) in the large- $x$  region at  $Q^2 > \mu^2$  as shown in Fig. 5 [38].

Next let us turn to the first moments (total polarizations)  $\Delta f(Q^2)$  of our polarized parton distributions, as defined in (1.3), and the resulting  $\Gamma_1^{p,n}(Q^2)$  in (1.5). It should be recalled that, in contrast to the LO, the first moments of the NLO (anti)quark densities do renormalize in the  $\overline{\text{MS}}$  scheme, i.e. are  $Q^2$  dependent (see, e.g., Ref. [1]), whereas the gluon polarization  $\Delta g(Q^2)$  renormalizes in both cases. Our LO ‘standard’ fit implies

$$\begin{aligned} \Delta u &= 0.871, & \Delta d &= -0.396, & \Delta\bar{q} &= \Delta s = \Delta\bar{s} = -0.054 \\ \Delta g(\mu_{\text{LO}}^2) &= 0.190, & \Delta g(5 \text{ GeV}^2) &= 0.684, & \Delta g(10 \text{ GeV}^2) &= 0.802 \end{aligned} \quad (2.7)$$



which result in  $\Delta\Sigma = 0.259$  and

$$\Gamma_1^p = 0.151, \quad \Gamma_1^n = -0.061. \quad (2.8)$$

Our NLO results are summarized in Table II at some typical values of  $Q^2$ . Both our LO and NLO results for  $\Gamma_1^{p,n}(Q^2)$  are in satisfactory agreement with recent experimental determinations [17 – 24]. Furthermore, due to the constraint (2.1), the Bjorken sum rule [39] holds manifestly in LO and, according to (1.5), the NLO  $\alpha_s$ -corrected sum rule reads

$$\Gamma_1^p(Q^2) - \Gamma_1^n(Q^2) = \frac{1}{6} g_A \left( 1 - \frac{\alpha_s(Q^2)}{\pi} \right). \quad (2.9)$$

It is also interesting to observe that at our low input scales  $Q^2 = \mu_{\text{LO,NLO}}^2 = 0.26, 0.40$  GeV<sup>2</sup> the nucleon's spin carried by the total helicities of quarks and gluons amounts only to

$$\begin{aligned} \frac{1}{2} \Delta\Sigma + \Delta g(\mu_{\text{LO}}^2) &\simeq 0.32 \\ \frac{1}{2} \Delta\Sigma(\mu_{\text{NLO}}^2) + \Delta g(\mu_{\text{NLO}}^2) &\simeq 0.35 \end{aligned} \quad (2.10)$$

which implies for the helicity sum rule (1.9) already a sizeable orbital contribution  $L_{q+g}(\mu_{\text{LO,NLO}}^2) \simeq 0.18, 0.15$  at the low input scales. Although this is in contrast to our somewhat more intuitive previous GRSV95 result [1],  $L_{q+g}(\mu_{\text{LO,NLO}}^2) \simeq 0$ , it should be kept in mind that, for the time being,  $\Delta g(Q^2)$  is rather weakly constrained by present data as was discussed above.

Finally, for completeness we have also performed a NLO analysis in a different factorization scheme, the so-called chirally invariant (CI) or JET scheme [8, 40, 41], but any other choice would do as well for studying the scheme dependence of our  $\overline{\text{MS}}$  fit results. Here, among other things [8, 40, 41], the total helicity of quarks,  $\Delta\Sigma_{\text{CI}}$ , is conserved, i.e.  $Q^2$ -independent, and is related to our  $\Delta\Sigma$  in the  $\overline{\text{MS}}$  scheme via

$$\Delta\Sigma(Q^2) = \Delta\Sigma_{\text{CI}} - 3 \frac{\alpha_s(Q^2)}{2\pi} \Delta g(Q^2)_{\text{CI}}. \quad (2.11)$$

Similarly agreeable fits as the ones in Figs. 1 – 3 can be obtained in this scheme, e.g. by choosing a large positive gluon density with a total (input) helicity  $\Delta g(\mu_{\text{NLO}}^2)_{\text{CI}} \simeq 0.6 - 0.7$  being about three times larger than in Table II and the sea density  $\delta\bar{q}_{\text{CI}}(\Delta\bar{q}_{\text{CI}})$  turns out to be roughly 50% smaller than the one of our best fit in the  $\overline{\text{MS}}$  ‘standard’ scenario; here the total quark helicity increases to  $\Delta\Sigma_{\text{CI}} \simeq 0.4$ .

### 3 $\text{SU}(3)_f$ broken ‘valence’ (broken–sea) scenario

The assumption of the flavor symmetric ‘standard’ scenario with its unbroken sea density in (2.5) is expected to be unrealistic, following our experience in the unpolarized case where a suppression of the strange sea component is required, as accomplished by the vanishing input  $s(x, \mu^2) = \bar{s}(x, \mu^2) = 0$  in GRV98 [25], in order to comply with experimental indications [42, 43] of an  $\text{SU}(3)_f$  broken sea, and the positivity constraint  $\delta s \leq s$ . Thus, in GRSV95 [1] we also considered a ‘valence’ scenario where, in contrast to (2.5),

$$\begin{aligned}\delta\bar{q}(x, \mu^2) &\equiv \delta\bar{u} = \delta\bar{d} = \delta u_{\text{sea}} = \delta d_{\text{sea}} \\ \delta s(x, \mu^2) &= \delta\bar{s}(x, \mu^2) = 0.\end{aligned}\tag{3.1}$$

Furthermore the full  $\text{SU}(3)_f$  flavor symmetry, giving rise to the constraints (2.1) and (2.2), is broken in the ‘valence’ scenario to the extent [44] that the flavor–changing hyperon  $\beta$ –decay data fix *only* the total helicity of *valence* quarks  $\Delta q_v \equiv \Delta q - \Delta\bar{q}$ :

$$\Delta u_v(\mu^2) - \Delta d_v(\mu^2) = F + D\tag{3.2}$$

$$\Delta u_v(\mu^2) + \Delta d_v(\mu^2) = 3F - D,\tag{3.3}$$

i.e.  $\Delta q_3 = \Delta u_v - \Delta d_v$  and  $\Delta q_8 = 3F - D + 4\Delta\bar{q}$  at  $Q^2 = \mu^2$  [1] according to (3.1). Therefore a light polarized sea  $\Delta\bar{q} < 0$  suffices here to account for the reduction of the Ellis–Jaffe estimate (2.4). This is the reason for our simplifying assumption of a maximally broken  $\text{SU}(3)_f$  strange sea input in (3.1) in order to reduce the number of input distributions

to be fitted to the rather scarce available polarization data, which are now sufficient for fixing these input distributions. (Future high-statistics data should allow, at least in principle, to extract the total strange sea polarization without employing any simplifying assumption, as for example from (1.8),  $\Delta(s + \bar{s}) = (\Delta\Sigma - \Delta q_8)/3$ .) The quality of the fits obtained is comparable to that of the ‘standard’ flavor-symmetric scenario discussed and presented in the previous Section, cf. Fig. 1. We refrain, however, from presenting these results here explicitly because the assumed remaining flavor-isospin symmetry of the light sea components in (3.1) appears to be somewhat artificial and unnatural in view of the flavor-asymmetric unpolarized light sea distributions  $\bar{d}(x, Q^2) > \bar{u}(x, Q^2)$  [25 – 28].

Turning now to the presumably more realistic scenario where also the *flavor-isospin symmetry of the polarized sea is broken*, we note, as already pointed out in the Introduction, that some model assumptions are needed for the corresponding input distributions. The analysis of the unpolarized structure functions yields

$$\bar{d}(x, \mu^2)/\bar{u}(x, \mu^2) \simeq u(x, \mu^2)/d(x, \mu^2), \quad (3.4)$$

which holds to a rather good accuracy for the GRV98 distributions [25]. This proportionality relation is expected to hold approximately at least for  $0.01 \lesssim x \lesssim 0.3$  where the breaking of the light sea  $\bar{d} > \bar{u}$  is directly tested experimentally via Drell–Yan dilepton production in  $pp$  and  $pd$  collisions [45] and semi-inclusive  $\pi^\pm$  production in  $ep$  and  $ed$  reactions [46]. The relation (3.4) may be considered [30] as a manifestation of the Pauli-blocking effect [47] which should be relevant also in the polarized parton sector. We therefore estimate the flavor-symmetry breaking of the polarized sea to be given in a first approximation by [30]

$$\delta\bar{d}(x, \mu^2)/\delta\bar{u}(x, \mu^2) = \delta u(x, \mu^2)/\delta d(x, \mu^2) \quad (3.5)$$

together with the previously advocated

$$\delta s(x, \mu^2) = \delta\bar{s}(x, \mu^2) = 0. \quad (3.6)$$

According to the unpolarized case above, we expect the proportionality relation (3.5) to hold approximately at least for  $0.01 \lesssim x \lesssim 0.3$ .

It should be reemphasized that, in complete analogy to unpolarized DIS, data on inclusive polarized DIS in kinematical regimes where only photon exchange is relevant give information only on the sums of quark and antiquark polarizations for each flavor,  $\delta q(x, Q^2) + \delta \bar{q}(x, Q^2)$ , appearing in  $g_1(x, Q^2)$  in (1.2). This implies, in particular, that the amount of flavor–SU(2) breaking in the polarized sea cannot be determined from such data since one can always change the parton densities by  $\delta q \rightarrow \delta q - \delta \phi_q$  and  $\delta \bar{q} \rightarrow \delta \bar{q} + \delta \phi_q$  for any arbitrary functions  $\delta \phi_u(x)$  and  $\delta \phi_d(x)$  *without* affecting at all the measured structure functions  $g_1^{p,n,d}(x, Q^2)$ . Restrictions on  $\delta \phi_q(x)$  occur only in our ‘valence’ scenario where  $\Delta \phi_d = -\Delta \phi_u$  for the first moments, as in general implied by our modified ( $\Delta \bar{u} \neq \Delta \bar{d}$ ) valence scenario constraints (3.7) and (3.8) below, and which have to even vanish for the ‘unbroken’ ( $\Delta \bar{u} = \Delta \bar{d}$ ) constraints (3.2) and (3.3). Therefore, for the time being, one has to resort to some, as far as possible, general and not too restrictive model assumptions concerning the breaking of the flavor–symmetry of the polarized light sea ( $\delta \bar{u} \neq \delta \bar{d}$ ), such as the proportionality (3.5). Only future polarized  $\vec{p}\vec{p}$  and  $\vec{p}\vec{d}$  Drell–Yan  $\mu^+\mu^-$  pair and weak vector boson production experiments [48] as well as polarized semi–inclusive DIS  $\vec{e}\vec{p}(\vec{d}) \rightarrow e(\pi, K)X$  experiments [49, 50] can provide us with direct measurements of the individual  $\delta \bar{u}(x, Q^2)$  and  $\delta \bar{d}(x, Q^2)$  distributions.

We now have, instead of (3.2),

$$\Delta q_3 = \Delta u_v(\mu^2) - \Delta d_v(\mu^2) + 2[\Delta \bar{u}(\mu^2) - \Delta \bar{d}(\mu^2)] = F + D, \quad (3.7)$$

and on account of (3.3) and (3.6)

$$\begin{aligned} \Delta q_8(\mu^2) &= \Delta u_v(\mu^2) + \Delta d_v(\mu^2) + 2[\Delta \bar{u}(\mu^2) + \Delta \bar{d}(\mu^2)] \\ &= 3F - D + 2[\Delta \bar{u}(\mu^2) + \Delta \bar{d}(\mu^2)] \\ &= \Delta \Sigma(\mu^2) \end{aligned} \quad (3.8)$$

where the imposed constraint (3.7) guarantees that the Bjorken sum rule (2.9) holds manifestly. Thus Eq. (1.5) becomes

$$\Gamma_1^{p,n}(Q^2) = \left[ \pm \frac{1}{12}(F + D) + \frac{5}{36}(3F - D) + \frac{10}{36}(\Delta\bar{u}(Q^2) + \Delta\bar{d}(Q^2)) \right] \left( 1 - \frac{\alpha_s(Q^2)}{\pi} \right) \quad (3.9)$$

apart from a marginal contribution  $\Delta s(Q^2) = \Delta\bar{s}(Q^2) < 0$  which is generated dynamically via the NLO evolution to  $Q^2 > \mu_{\text{NLO}}^2$  even for the vanishing input in (3.6). Thus, in this case, only the *total* light–quark sea contribution in (3.9) has to be *negative*,  $\Delta\bar{u}(Q^2) + \Delta\bar{d}(Q^2) < 0$ , in order to achieve the experimentally required reduction of the Ellis–Jaffe expectation (2.4).

Our resulting input distributions can be parametrized as in (2.6) where now, instead of the unbroken  $\delta\bar{q}$  sea, we have a similar parametrization for  $\delta\bar{u}(x, \mu^2)$  and  $\delta\bar{d}(x, \mu^2)$  which are constrained by (3.5) [51], together with the respective flavor–broken unpolarized input densities  $\bar{u}(x, \mu^2)$  and  $\bar{d}(x, \mu^2)$  taken from [25]. The parameters of our optimal LO densities at  $\mu_{\text{LO}}^2 = 0.26 \text{ GeV}^2$  and the ones of the NLO( $\overline{\text{MS}}$ ) densities at  $\mu_{\text{NLO}}^2 = 0.40 \text{ GeV}^2$  are given in Table III. These optimal fits correspond to  $\chi_{\text{DF,LO}}^2 = 0.823$  and  $\chi_{\text{DF,NLO}}^2 = 0.816$  similarly to the ‘standard’ scenario in Sec. 2. The quality of these LO and NLO fits to  $A_1^N(x, Q^2)$  in the broken ‘valence’ scenario is practically identical to our new fit in the ‘standard’ scenario shown in Fig. 1 by the solid curves. The same holds true also for  $g_1^{p,n,d}(x, Q^2)$  shown in Figs. 2 and 3. The corresponding LO and NLO parton distributions at the respective input scales  $Q^2 = \mu_{\text{LO,NLO}}^2$  in Eq. (2.6) [51] with the ‘valence’ scenario fit parameters given in Table III are shown in Fig. 6, which are also compared with our reference unpolarized valence–like dynamical input densities of [25] which satisfy the positivity constraint  $|\delta f| \leq f$ . The polarized gluon densities turn out to be somewhat larger here, in particular in NLO, than the ones in the ‘standard’ scenario shown in Fig. 4. It should be furthermore emphasized that we always expect for the broken light–sea input densities to have a *positive*  $\delta\bar{u}$  and a *negative*  $\delta\bar{d}$  with  $|\delta\bar{d}| > \delta\bar{u}$ , i.e.  $\delta\bar{u} - \delta\bar{d} > 0$  and  $\delta\bar{u} + \delta\bar{d} < 0$ .

In Fig. 7 we present the flavor asymmetry  $x(\delta\bar{u}-\delta\bar{d})(x, \mu^2)$  separately, as obtained from Fig. 6, which compares favorably with predictions of the relativistic field theoretical chiral quark–soliton model [52, 50]. Similar results have been obtained by a recent analysis [53] based on the statistical parton model which are supposed to hold at a somewhat larger input scale  $Q_0^2 = M_p^2 \simeq 0.9 \text{ GeV}^2$ . We note furthermore that the prediction  $\delta g(x, M_p^2) = 0$  of this latter model is consistent with the results of the present analysis which do *not* exclude this possibility, cf. Fig. 3. The resulting NLO distributions at  $Q^2 = 5 \text{ GeV}^2$  are shown in Fig. 8 where they are also compared with our new NLO results obtained in the ‘standard’ scenario as shown by the solid curves in Fig. 5.

The first moments (total polarizations)  $\Delta f(Q^2)$  of the polarized parton distributions of our fully flavor–broken ‘valence’ scenario and the resulting  $\Gamma_1^{p,n}(Q^2)$  are in LO given by

$$\begin{aligned} \Delta u = 0.664, \quad \Delta d = -0.248, \quad \Delta\bar{u} = 0.093, \quad \Delta\bar{d} = -0.261, \quad \Delta s = \Delta\bar{s} = 0 \\ \Delta g(\mu_{\text{LO}}^2) = 0.300, \quad \Delta g(5 \text{ GeV}^2) = 0.963, \quad \Delta g(10 \text{ GeV}^2) = 1.122 \end{aligned} \quad (3.10)$$

which result in  $\Delta\Sigma = 0.248$  and

$$\Gamma_1^p = 0.140, \quad \Gamma_1^n = -0.071. \quad (3.11)$$

Our NLO results are summarized in Table IV at some typical values of  $Q^2$ . The nucleon’s spin is carried almost entirely by the total helicities of quarks and gluons at the LO and NLO input scales

$$\frac{1}{2}\Delta\Sigma(\mu_{\text{LO,NLO}}^2) + \Delta g(\mu_{\text{LO,NLO}}^2) \simeq 0.42, \quad 0.48 \quad (3.12)$$

which is larger than the ‘standard’ scenario results (2.10), and thus a very small orbital contribution  $L_{q+g}(\mu_{\text{LO,NLO}}^2) \simeq 0.08, 0.02$  is required at the low input scales in order to comply with the sum rule (1.9). This is somewhat similar to our previous results [1], but again  $\Delta g(Q^2)$  is not strongly constrained by present data. Nevertheless it is intuitively appealing that this nonperturbative orbital (angular momentum) contribution to the helicity sum rule (1.9) vanishes at our low input scales,  $L_{q+g}(\mu^2) \simeq 0$ . This is in

contrast to larger scales  $Q^2 > \mu^2$  where hard radiative effects give rise to sizeable orbital components due to the increasing  $k_T$  of the partons, which eventually have to compensate in (1.9) the strongly increasing gluon polarization  $\Delta g(Q^2) \sim \alpha_s^{-1}(Q^2)$ : in both scenarios we obtain, for example,  $\Delta g(10 \text{ GeV}^2) \simeq 1$ .

Finally let us conclude with a few remarks concerning the flavor–symmetry breaking which was implemented in our broken ‘valence’ scenario via the entirely empirical relation (3.5). On rather general grounds one expects the product

$$\delta q(x, \mu^2) \delta \bar{q}(x, \mu^2) \equiv P(x) \quad (3.13)$$

to be a universal flavor–*independent* function  $P(x)$ , since the effect of Pauli–blocking is only related to the spin (helicities) of quarks and antiquarks irrespective of their flavor degree of freedom. This implies  $\delta u(x, \mu^2) \delta \bar{u}(x, \mu^2) = \delta d(x, \mu^2) \delta \bar{d}(x, \mu^2)$ , i.e. Eq. (3.5). Furthermore, we have seen that the data select, within our ‘valence’ scenario with its totally flavor–broken polarized light sea densities in (3.5) and (3.6), the solution of Eq. (3.5) which satisfies  $P(x) > 0$  in (3.13) for  $q = u, d$  as can be seen in Fig. 6. This can be understood [30] as a consequence of the expected predominant *pseudoscalar* configuration [29, 54] of the quark–antiquark pairs in the nucleon sea. In fact, the two relations  $u\bar{u} \simeq d\bar{d}$  and  $\delta u \delta \bar{u} = \delta d \delta \bar{d}$  at the input scale  $Q^2 = \mu^2$  can be rewritten as

$$\begin{aligned} P_p(x) &\equiv u_+ \bar{u}_+ + u_- \bar{u}_- \simeq d_+ \bar{d}_+ + d_- \bar{d}_- \\ P_a(x) &\equiv u_+ \bar{u}_- + u_- \bar{u}_+ \simeq d_+ \bar{d}_- + d_- \bar{d}_+ \end{aligned} \quad (3.14)$$

with  $P = P_p - P_a$  in (3.13) and the common helicity densities being given by  $\binom{(-)}{q}_{\pm} = (\binom{(-)}{q} \pm \delta \binom{(-)}{q})/2$  where for brevity we have dropped the  $x$ –dependence. A predominant pseudoscalar configuration of  $(q\bar{q})$ –pairs in the nucleon sea implies, via Pauli–blocking, that the aligned quark–quark configurations  $q_+(q_+\bar{q}_-)$  and  $q_-(q_-\bar{q}_+)$  are suppressed relatively to the antialigned  $q_+(q_-\bar{q}_+)$  and  $q_-(q_+\bar{q}_-)$  ‘cloud’ configurations, i.e.  $P_p(x) > P_a(x)$  which implies  $P(x) > 0$  in (3.13). The result for  $P_p/P_a$ , corresponding to our optimal fit, is shown in Fig. 9: clearly, this ratio will be maximal where  $xq(x, \mu^2)$  and  $x\delta q(x, \mu^2)$  are

maximal at  $x \simeq 0.2 - 0.4$ , cf. Fig. 6, i.e. where the Pauli-blocking, Eq. (3.13), is most effective which is nicely exhibited in Fig. 9 in LO and NLO.

It is interesting to mention that some of these expectations, which derive mainly from our light-sea flavor breaking relation (3.5), have been already confirmed by a recent entirely independent simultaneous analysis [14] of polarized DIS and semi-inclusive deep inelastic scattering (SIDIS) asymmetry-data. In particular the more recent high precision SIDIS HERA-HERMES data [55] on  $h^+$  production ( $h = \pi, K$  dominantly) off a proton target,  $e\vec{p} \rightarrow eh^+X$ , seem to play a decisive role in favoring flavor-broken light sea densities  $\delta\bar{u}(x, Q^2) \neq \delta\bar{d}(x, Q^2)$ , despite the fact that these asymmetry data on  $A_{1p}^{h^+}$  refer to rather small scales  $Q^2 \gtrsim 1 \text{ GeV}^2$ . The reason for this discriminative power is, when combined with the data from inclusive DIS, due to the fact that  $A_{1p}^{h^+}$  is proportional [14], besides to the dominant valence contribution, also to  $\delta\bar{d} - 4\delta\bar{u}$ , multiplied by a ‘favored’ fragmentation function, which is significantly more sensitive to  $\delta\bar{u}$  than to  $\delta\bar{d}$ . A clear preference for a *positive*  $\delta\bar{u}$  has been observed [14], which is very similar to our NLO  $\delta\bar{u}$  shown in Fig. 6(b), and a flavor symmetric ‘standard’ light sea scenario seems to be strongly disfavored.

We have calculated at NLO the spin asymmetries for semi-inclusive DIS using the well known theoretical SIDIS framework [56, 14] together with our results for the polarized parton distributions of the ‘standard’ and ‘valence’ scenario with their flavor-symmetric and flavor-broken light sea densities, respectively, employing the fragmentation functions of [57]. (We did not use the alternative set of recent fragmentation functions suggested in [58], since they refer to scales  $Q^2$  larger than  $2 \text{ GeV}^2$ .) The results for the relevant SIDIS asymmetry  $A_{1p}^{h^+}$  are shown in Fig. 10. Although the high precision HERMES data [55] seem to favor slightly the ‘valence’ scenario with its flavor-broken light sea, the results of the ‘standard’ scenario with its flavor-symmetric light sea cannot yet be ruled out. Both scenarios in Fig. 10 give rise to a comparable  $\chi^2/(9 \text{ data points})$  of 7.6 and 8.5 for the ‘valence’ and ‘standard’ scenario, respectively.



## 4 Summary and conclusions

All recent polarized DIS data, including the most recent SLAC-E155 proton data [24], have been analyzed and studied within the ‘standard’ and ‘valence’ scenario in LO and NLO of QCD. The ‘standard’ scenario, characterized by (2.1) and (2.2), refers to the common simplified, but probably unrealistic, assumption of an  $SU(3)_f$  flavor-symmetric polarized light sea. The original ‘valence’ scenario [1], characterized by (3.2) and (3.3), is now modified by employing a *totally*  $SU(3)_f$  asymmetric polarized light sea  $\delta\bar{u} \neq \delta\bar{d} \neq \delta\bar{s}$  which leads to the modified constraints (3.7) and (3.8). Since inclusive polarized DIS data cannot fix the flavor-broken sea densities, we have modelled the flavor-asymmetric light sea densities  $\delta\bar{u} \neq \delta\bar{d}$  using a Pauli-blocking ansatz [30] in (3.5), because similar ‘blocking’ effects can also explain the flavor-asymmetry of unpolarized sea densities ( $\bar{d} > \bar{u}$ ). All our resulting polarized parton distributions respect the fundamental positivity constraints down to the low resolution scales  $Q^2 = \mu_{\text{LO}}^2 = 0.26 \text{ GeV}^2$  and  $\mu_{\text{NLO}}^2 = 0.40 \text{ GeV}^2$ . The polarized gluon distribution  $\delta g(x, Q^2)$  is weakly constrained by present data in both scenarios. In particular, a vanishing gluon input  $\delta g(x, \mu^2) = 0$  is equally compatible with all present measurements of  $A_1^N(x, Q^2)$  or  $g_1^N(x, Q^2)$ . Only a fully saturated (via the positivity constraint) gluon input  $\delta g(x, \mu^2) = \pm g(x, \mu^2)$  appears to be disfavored by present data.

The presumably more realistic ‘valence’ scenario with its flavor-broken light sea quark distributions  $\delta\bar{u} \neq \delta\bar{d} (\neq \delta\bar{s} = \delta s \simeq 0)$  leads to a *positive*  $\delta\bar{u}(x, Q^2)$  density and a sizeably larger negative  $\delta\bar{d}(x, Q^2)$ . These results are supported by a recent combined analysis [14] of polarized DIS and semi-inclusive DIS data and agree with predictions of the relativistic field theoretical chiral quark-soliton model [52, 50] and of the statistical parton model [53]. Present high statistics HERA-HERMES data [55] on semi-inclusive asymmetries  $A_{1\text{N}}^{h^\pm}$  for  $h^\pm$  production off nucleon targets cannot, however, yet uniquely discriminate between our ‘valence’ scenario with flavor-broken polarized light sea densities and the

common ‘standard’ scenario with a flavor–symmetric light sea–quark distribution.

A FORTRAN package containing our optimally fitted ‘standard’ and fully flavor–broken ‘valence’ NLO( $\overline{\text{MS}}$ ) as well as LO distributions can be obtained by electronic mail.

## **Acknowledgements**

We are grateful to Greg Mitchell for useful information concerning the recent E155 proton data. This work has been supported in part by the ‘Bundesministerium für Bildung, Wissenschaft, Forschung und Technologie’ and the ‘Deutsche Forschungsgemeinschaft’, Berlin/Bonn. W.V. is grateful to RIKEN, Brookhaven National Laboratory and the U.S. Department of Energy (contract number DE-AC02-98CH10886) for providing the facilities essential for the completion of his work.

## References

- [1] M. Glück, E. Reya, M. Stratmann, and W. Vogelsang, *Phys. Rev.* **D53**, 4775 (1996).
- [2] T. Gehrmann and W.J. Stirling, *Phys. Rev.* **D53**, 6100 (1996).
- [3] R.D. Ball, S. Forte, and G. Ridolfi, *Phys. Lett.* **B378**, 255 (1996);  
G. Altarelli, R.D. Ball, S. Forte, and G. Ridolfi, *Nucl. Phys.* **B496**, 337 (1997); *Acta Phys. Pol.* **B29**, 1145(1998).
- [4] K. Abe et al., SLAC-E154 Collab., *Phys. Lett.* **B405**, 180 (1997).
- [5] B. Adeva et al., CERN-SM Collab., *Phys. Rev.* **D58**, 112002 (1998).
- [6] C. Bourrely, F. Buccella, O. Pisanti, P. Santorelli, and J. Soffer, *Prog. Theor. Phys.* **99**, 1017 (1998).
- [7] D. de Florian, O.A. Sampayo, and R. Sassot, *Phys. Rev.* **D57**, 5803 (1998).
- [8] E.A. Leader, A.V. Sidorov, and D.B. Stamenov, *Int. J. Mod. Phys.* **A13**, 5573 (1998);  
*Phys. Rev.* **D58**, 114028 (1998); *Phys. Lett.* **B445**, 232 (1998); **B462**, 189 (1999);  
*Phys. Lett.* **B488**, 283 (2000).
- [9] L.E. Gordon, M. Goshtasbpour, and G.P. Ramsey, *Phys. Rev.* **D58**, 094017 (1998).
- [10] S. Incerti and F. Sabatie, SLAC-E154/155 Collab., CEA–Saclay PCCF-RI-9901 (1999).
- [11] S. Tatur, J. Bartelski, and M. Kurzela, *Acta. Phys. Pol.* **B31**, 647 (2000);  
J. Bartelski and S. Tatur, hep-ph/0004251 (2000).
- [12] D.K. Ghosh, S. Gupta, and D. Indumathi, *Phys. Rev.* **D62**, 094012 (2000).
- [13] Y. Goto et al., Asymmetry Analysis Collab., *Phys. Rev.* **D62**, 034017 (2000).
- [14] D. de Florian and R. Sassot, *Phys. Rev.* **D62**, 094025 (2000).

- [15] SLAC–Yale E80 Collaboration, M.J. Alguard et al., *Phys. Rev. Lett.* **37**, 1261 (1976);  
G. Baum et al., *ibid.* **45**, 2000 (1980);  
SLAC–Yale–E130 Collaboration, G. Baum et al., *Phys. Rev. Lett.* **51**, 1135 (1983).
- [16] CERN–EM Collaboration, J. Ashman et al., *Phys. Lett.* **B206**, 364 (1988); *Nucl. Phys.* **B328**, 1 (1989).
- [17] CERN–SM Collaboration, B. Adeva et al., *Phys. Rev.* **D58**, 112001 (1998).
- [18] SLAC–E143 Collaboration, K. Abe et al., *Phys. Rev.* **D58**, 120003 (1998).
- [19] SLAC–E142 Collaboration, P.L. Anthony et al., *Phys. Rev.* **D54**, 6620 (1996).
- [20] DESY–HERMES Collaboration, K. Ackerstaff et al., *Phys. Lett.* **B404**, 383 (1997).
- [21] DESY–HERMES Collaboration, A. Airapetian et al., *Phys. Lett.* **B442**, 484 (1998).
- [22] SLAC–E154 Collaboration, K. Abe et al., *Phys. Rev. Lett.* **79**, 26 (1997).
- [23] SLAC–E155 Collaboration, P.L. Anthony et al., *Phys. Lett.* **B463**, 339 (1999).
- [24] SLAC–E155 Collaboration, P.L. Anthony et al., SLAC–PUB–7994, July 2000 T/E (hep–ph/0007248).
- [25] M. Glück, E. Reya, and A. Vogt, *Eur. Phys. J.* **C5**, 461 (1998).
- [26] A.D. Martin, R.G. Roberts, W.J. Stirling, and R.S. Thorne, *Eur. Phys. J.* **C4**, 463 (1998); *Eur. Phys. J.* **C14**, 133 (2000).
- [27] H.L. Lai et al., CTEQ5 Collab., *Eur. Phys. J.* **C12**, 375 (2000).
- [28] H. Botje, *Eur. Phys. J.* **C14**, 285 (2000).
- [29] For recent reviews see, for example, S. Kumano, *Phys. Rep.* **303**, 183 (1998);  
J. Speth and A.W. Thomas, *Adv. Nucl. Phys.* **24**, 83 (1998).

- [30] M. Glück and E. Reya, *Mod. Phys. Lett.* **A15**, 883 (2000) (hep-ph/0002182).
- [31] W. Furmanski and R. Petronzio, *Z. Phys.* **C11**, 293 (1982).
- [32] M. Glück, E. Reya, and W. Vogelsang, *Nucl. Phys.* **B351**, 579 (1991).
- [33] Particle Data Group, C. Caso et al., *Eur. Phys. J.* **C3**, 1 (1998).
- [34] M. Karliner and H.J. Lipkin, *Phys. Lett.* **B461**, 280 (1999).
- [35] J. Ellis and R.L. Jaffe, *Phys. Rev.* **D9**, 1444 (1974); **10**, 1669 (E) (1974);  
M. Gourdin, *Nucl. Phys.* **B38**, 418 (1972).
- [36] S.J. Brodsky and I. Schmidt, *Phys. Lett.* **B234**, 144 (1990); S.J. Brodsky,  
M. Burkardt, and I. Schmidt, *Nucl. Phys.* **B441**, 197 (1995);  
F.E. Close and D. Sivers, *Phys. Rev. Lett.* **39**, 1116 (1977).
- [37] Note that our ansatz violates (slightly) the ‘helicity retention’ concept developed in Ref. [36], by which  $\delta f(x, Q^2)/f(x, Q^2) \rightarrow 1$  for  $x \rightarrow 1$ . Such relations follow in perturbative QCD and need not necessarily be fulfilled by our non-perturbative input at  $Q^2 = \mu^2$ . In any case, we could always appropriately modify our ansatz at very high  $x$  so as to satisfy the ‘helicity retention’ conditions. Enforcing in our fits all  $\beta_f$  to vanish in Eq. (2.6) increases the total  $\chi^2$  by several units, giving rise to worse fits than our optimal ones.
- [38] We have refrained from attempting to extract information from measurements of the spin asymmetry for photoproduction of oppositely charged hadron-pairs presented by the HERMES collaboration [A. Airapetian et al., *Phys. Rev. Lett.* **84**, 2584 (2000)]. Such data could in principle constrain the spin gluon density  $\delta g(x, Q^2)$ ; however, the smallness of the hadron transverse momenta accessed in this experiment makes an interpretation of the data in terms of QCD hard scattering difficult. In fact, as stated by the HERMES collaboration, their published gluon asymmetry

$\delta g(x, Q^2)/g(x, Q^2) = 0.41 \pm 0.18$  at  $x \simeq 0.17$  and  $Q^2 \equiv \langle p_T^2 \rangle = 2.1 \text{ GeV}^2$ , which implies  $x\delta g(x, Q^2) \simeq 0.35 \pm 0.15$ , actually compatible with our results in Fig. 5, does not include systematic theoretical errors. These could be sizeable in the low transverse momentum region considered.

- [39] J.D. Bjorken, *Phys. Rev.* **148**, 1467 (1966); *ibid.* **D1**, 1376 (1970).
- [40] H.Y. Cheng, *Int. J. Mod. Phys.* **A11** (1996) 5109; *Phys. Lett.* **B427** (1998) 371.  
The explicit transformation of the splitting functions (anomalous dimensions) and coefficient functions from the  $\overline{\text{MS}}$  to the CI (JET) scheme can be found in this latter reference as well as in the third reference of [8].
- [41] D. Müller and O.V. Teryaev, *Phys. Rev.* **D56**, 2607 (1997).
- [42] H. Abramowicz et al., CDHSW Collab., *Z. Phys.* **C15**, 19 (1982).
- [43] CCFR Collab., C. Foudas et al., *Phys. Rev. Lett.* **64**, 1207 (1990);  
S.A. Rabinowitz et al., *ibid.* **70**, 134 (1993); A.O. Bazarko et al., *Z. Phys.* **C65**, 189 (1995).
- [44] H.J. Lipkin, *Phys. Lett.* **B256**, 284 (1991); **337**, 157 (1994);  
J. Lichtenstadt and H.J. Lipkin, *ibid.* **353**, 119 (1995).
- [45] A. Baldit et al., NA51 Collab., *Phys. Lett.* **B332**, 244 (1994);  
E.A. Hawker et al., E866 Collab., *Phys. Rev. Lett.* **80**, 3715 (1998).
- [46] C.A. Miller, HERMES Collab., Proceedings of DIS '99, *Nucl Phys. B* (Proc. Suppl.) **79**, 146 (1999).
- [47] R.D. Field and R.P. Feynman, *Phys. Rev.* **D15**, 2590 (1977).
- [48] S. Kumano and M. Miyama, *Phys. Lett.* **B479**, 149 (2000);  
B. Dressler et al., Univ. Bochum RUB-TPII-13/99 (hep-ph/9910464);

- C. Bourrely and J. Soffer, *Phys. Lett.* **B314**, 132 (1993); *Nucl. Phys.* **B423**, 329 (1994).
- [49] T. Morii and T. Yamanishi, *Phys. Rev.* **D61**, 057501 (2000).
- [50] B. Dressler et al., *Eur. Phys. J.* **C14**, 147 (2000).
- [51] The easiest and consistent way to implement directly (even for Mellin- $n$  moments) the constraint (3.5) in a fit routine is to fit, for example,  $\delta u$ ,  $\delta d$  and  $\delta \bar{u}$  according to the ansatz (2.6) which fix  $\delta \bar{d}(x, \mu^2)$  via (3.5) and (3.4):  $\delta \bar{d}/\bar{d} \simeq (\delta u/u) (\delta \bar{u}/\bar{u})/(\delta d/d)$  where the unpolarized densities are taken from Ref. [25]. Thus  $N_{\bar{d}} = N_u N_{\bar{u}}/N_d$ ,  $\alpha_{\bar{d}} = \alpha_u + \alpha_{\bar{u}} - \alpha_d$  and  $\beta_{\bar{d}} = \beta_u + \beta_{\bar{u}} - \beta_d$ .
- [52] D. Diakonov et al., *Nucl. Phys.* **B480**, 341 (1996); *Phys. Rev.* **D56**, 4069 (1997); M. Wakamatsu and T. Kubota, *Phys. Rev.* **D60**, 034020 (1999); K. Goeke et al., Univ. Bochum RUB-TPII-18/99 (hep-ph/0001272).
- [53] R.S. Bhalerao, *Phys. Lett.* **B380**, 1 (1996); **387**, 881 (E) (1996); talk given at the Int. Conf. on QNP 2000, Adelaide, Feb. 2000, *Nucl. Phys.* **A680**, 62 (2000); R.S. Bhalerao, N.G. Kelkar, and B. Ram, *Phys. Lett.* **B476**, 285 (2000).
- [54] N.N. Nikolaev et al., *Phys. Rev.* **D60**, 014004 (1999).
- [55] K. Ackerstaff et al., HERMES Collab., *Phys. Lett.* **B464**, 123 (1999).
- [56] D. de Florian, C.A. Garcia Canal and R. Sassot, *Nucl. Phys.* **B470**, 195 (1996).
- [57] S. Kretzer, *Phys. Rev.* **D62**, 054001 (2000).
- [58] B.A. Kniehl, G. Kramer and B. Pötter, *Nucl. Phys.* **B582**, 514 (2000).

**Table I.** The parameters of the LO and NLO input parton distributions, as defined in Eq. (2.6), at  $\mu_{\text{LO}}^2 = 0.26 \text{ GeV}^2$  and  $\mu_{\text{NLO}}^2 = 0.40 \text{ GeV}^2$ , respectively, for the ‘standard’ scenario as obtained from fits to the data in [15 – 24].

	standard scenario	
	LO	NLO
$N_u$	0.851	1.019
$\alpha_u$	0.45	0.52
$\beta_u$	0	0.12
$N_d$	-0.734	-0.669
$\alpha_d$	0.49	0.43
$\beta_d$	0.03	0
$N_{\bar{q}}$	-0.587	-0.272
$\alpha_{\bar{q}}$	0.68	0.38
$\beta_{\bar{q}}$	0	0
$N_s$	1	1
$N_g$	1.669	1.419
$\alpha_g$	1.79	1.43
$\beta_g$	0.15	0.15
$\chi^2/209$ data pts.	174.9	169.8

**Table II.** First moments (total polarizations)  $\Delta f$  of polarized NLO parton densities  $\delta f(x, Q^2)$  and  $g_1^{p,n}(x, Q^2)$ , defined in (1.3) and (1.4), as obtained in the ‘standard’ scenario. The marginal differences between  $\Delta \bar{u}$  and  $\Delta \bar{d}$  at  $Q^2 > \mu^2$ , generated dynamically by the NLO evolution, are not displayed.

$Q^2 (\text{GeV}^2)$	$\Delta u$	$\Delta d$	$\Delta \bar{q}$	$\Delta g$	$\Delta \Sigma$	$\Gamma_1^p$	$\Gamma_1^n$
$\mu_{\text{NLO}}^2$	0.863	-0.404	-0.062	0.240	0.211	0.119	-0.054
1	0.861	-0.405	-0.063	0.420	0.204	0.127	-0.058
5	0.859	-0.406	-0.064	0.708	0.197	0.132	-0.062
10	0.859	-0.406	-0.064	0.828	0.197	0.133	-0.063



**Table III.** The parameters of the LO and NLO input distributions, as defined in Eq. (2.6), with  $\bar{q}$  to be identified with  $\bar{u}$ , at  $\mu_{\text{LO}}^2 = 0.26 \text{ GeV}^2$  and  $\mu_{\text{NLO}}^2 = 0.40 \text{ GeV}^2$ , respectively, for the ‘valence’ scenario. We have fitted the broken light–sea input density  $\delta\bar{u}(x, \mu^2)$  and fixed  $\delta\bar{d}(x, \mu^2)$  via (3.5) and (3.4) [51].

	valence scenario	
	LO	NLO
$N_u$	1.297	2.043
$\alpha_u$	0.79	0.97
$\beta_u$	0.27	0.64
$N_d$	-2.496	-2.709
$\alpha_d$	1.17	1.26
$\beta_d$	1.31	1.06
$N_{\bar{u}}$	2.005	1.727
$\alpha_{\bar{u}}$	0.79	0.73
$\beta_{\bar{u}}$	1.93	2.00
$N_s$	0	0
$N_g$	6.637	20.45
$\alpha_g$	2.00	2.92
$\beta_g$	1.50	1.68
$\chi^2/209 \text{ data pts.}$	172.0	170.5

**Table IV.** First moments (total polarizations)  $\Delta f$  of polarized parton densities  $\delta f(x, Q^2)$  and  $g_1^{p,n}(x, Q^2)$ , defined in (1.3) and (1.4), as obtained in the fully flavor–broken ‘valence’ scenario. The marginal finite  $\Delta s = \Delta\bar{s}(Q^2 > \mu_{\text{NLO}}^2)$  are generated dynamically by the NLO evolution.

$Q^2 \text{ (GeV}^2\text{)}$	$\Delta u$	$\Delta d$	$\Delta\bar{u}$	$\Delta\bar{d}$	$\Delta s = \Delta\bar{s}$	$\Delta g$	$\Delta\Sigma$	$\Gamma_1^p$	$\Gamma_1^n$
$\mu_{\text{NLO}}^2$	0.693	-0.255	0.087	-0.232	0	0.330	0.293	0.119	-0.053
1	0.691	-0.257	0.086	-0.234	$-1.95 \times 10^{-3}$	0.579	0.282	0.127	-0.058
5	0.689	-0.258	0.085	-0.235	$-3.31 \times 10^{-3}$	0.974	0.273	0.132	-0.062
10	0.688	-0.258	0.085	-0.236	$-3.64 \times 10^{-3}$	1.140	0.272	0.133	-0.062

## Figure Captions

- Fig. 1.** Comparison of our NLO results for  $A_1^N(x, Q^2)$  as obtained from the fitted input at  $Q^2 = \mu_{\text{NLO}}^2$  for the ‘standard’  $SU(3)_f$  flavor-symmetric sea scenario [Eq. (2.6) and Table I] with present data [16 – 24]. The  $Q^2$  values adopted here correspond to the different values quoted in [16 – 24] for each data point starting at  $Q^2 \geq 1 \text{ GeV}^2$  at the lowest available  $x$  bin. Our old NLO GRSV95 fit [1] is shown for comparison as well (dashed curves). Our present LO fit is very similar to the NLO one shown by the solid curves.
- Fig. 2.** Comparing the  $Q^2$ -dependence of our LO and NLO ‘standard’ scenario results with recent data [16 – 18, 21, 24] on  $g_1^p(x, Q^2)$ . To ease the graphical representation we have multiplied all results at the various fixed values of  $x$  by the numbers indicated in parentheses.
- Fig. 3.** The  $x$ -dependence of  $g_1^N$  at  $Q^2 = 5 \text{ GeV}^2$  in the NLO ‘standard’ scenario. Different choices of the gluon input  $\delta g(x, \mu_{\text{NLO}}^2)$  in (2.6) are shown by the dashed and dotted curves as indicated. Allowing our optimal total  $\chi^2$  to change by one unit,  $\delta\chi^2 = \pm 1$ , results in the shaded areas shown. The data are taken from [17, 18, 20, 22 – 24].
- Fig. 4.** (a) Comparison of our fitted ‘standard’ LO input distributions in Eq. (2.6) and Table I at  $\mu_{\text{LO}}^2 = 0.26 \text{ GeV}^2$  with our previous old GRSV95 fit [1] and with the unpolarized dynamical GRV98 input densities of [25]. (b) The same as in (a) but for the NLO input densities at  $\mu_{\text{NLO}}^2 = 0.40 \text{ GeV}^2$ .
- Fig. 5.** The polarized LO and NLO( $\overline{\text{MS}}$ ) distributions at  $Q^2 = 5 \text{ GeV}^2$  in the ‘standard’ scenario, as obtained from the input densities at  $Q^2 = \mu_{\text{LO, NLO}}^2$  in Fig. 4. Our old NLO results [1] are shown for comparison.
- Fig. 6.** (a) Comparison of our fitted fully broken ‘valence’ scenario LO input distributions in Eq. (2.6) [51] and Table III at  $\mu_{\text{LO}}^2 = 0.26 \text{ GeV}^2$  with the unpolarized GRV98

input densities of [25]. **(b)** The same as in (a) but for the NLO input densities at  $\mu_{\text{NLO}}^2 = 0.40 \text{ GeV}^2$ .

**Fig. 7.** LO and NLO results for the difference of the broken light–sea input densities  $\delta\bar{u}(x, \mu^2)$  and  $\delta\bar{d}(x, \mu^2)$  in the ‘valence’ scenario as obtained from Fig. 6. The prediction of the chiral quark–soliton model is taken from K. Goeke et al. [52].

**Fig. 8.** The polarized LO and NLO( $\overline{\text{MS}}$ ) distributions at  $Q^2 = 5 \text{ GeV}^2$  in the fully flavor–broken ‘valence’ scenario, as obtained from the input densities at  $Q^2 = \mu_{\text{LO,NLO}}^2$  in Fig. 6. For comparison the new NLO results of the ‘standard’ (unbroken sea) scenario are shown as well by the dashed curves (which coincide with the solid curves of Fig. 5.).

**Fig. 9.** The ratio of  $P_p(x)$  and  $P_a(x)$ , defined in (3.14), at the LO and NLO input scales  $\mu_{\text{LO,NLO}}^2$  which demonstrates the Pauli–blocking of the disfavored antiparallel  $q_{\pm}\bar{q}_{\mp}$  configurations relative to the favored parallel  $q_{\pm}\bar{q}_{\pm}$  configurations as discussed in the text.

**Fig. 10.** NLO predictions for the semi–inclusive DIS asymmetry  $A_{1p}^{h^+}$  for  $h^+$  production off a proton target within the ‘valence’ and ‘standard’ scenario. The HERMES data are taken from [55].

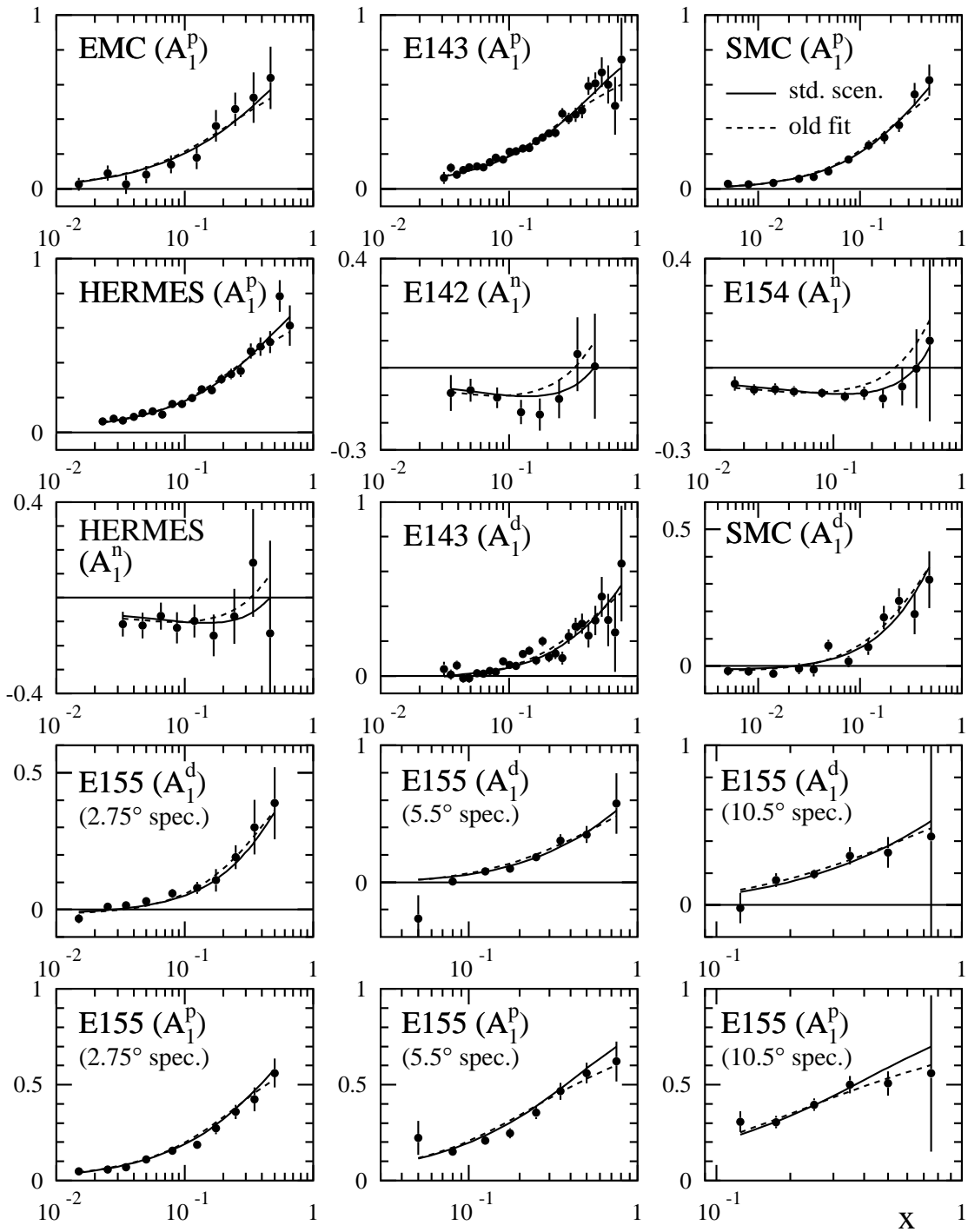


Fig. 1

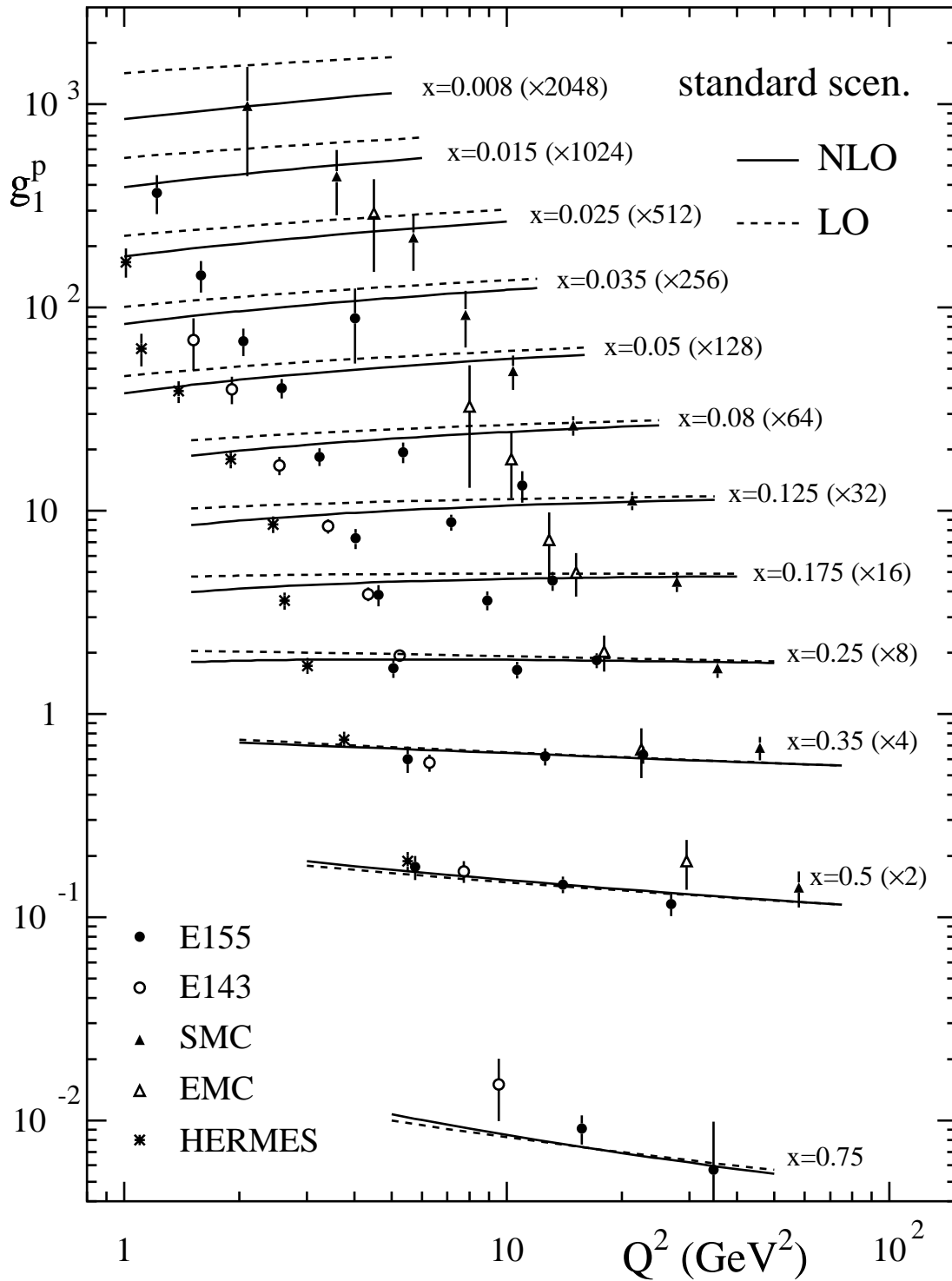


Fig. 2

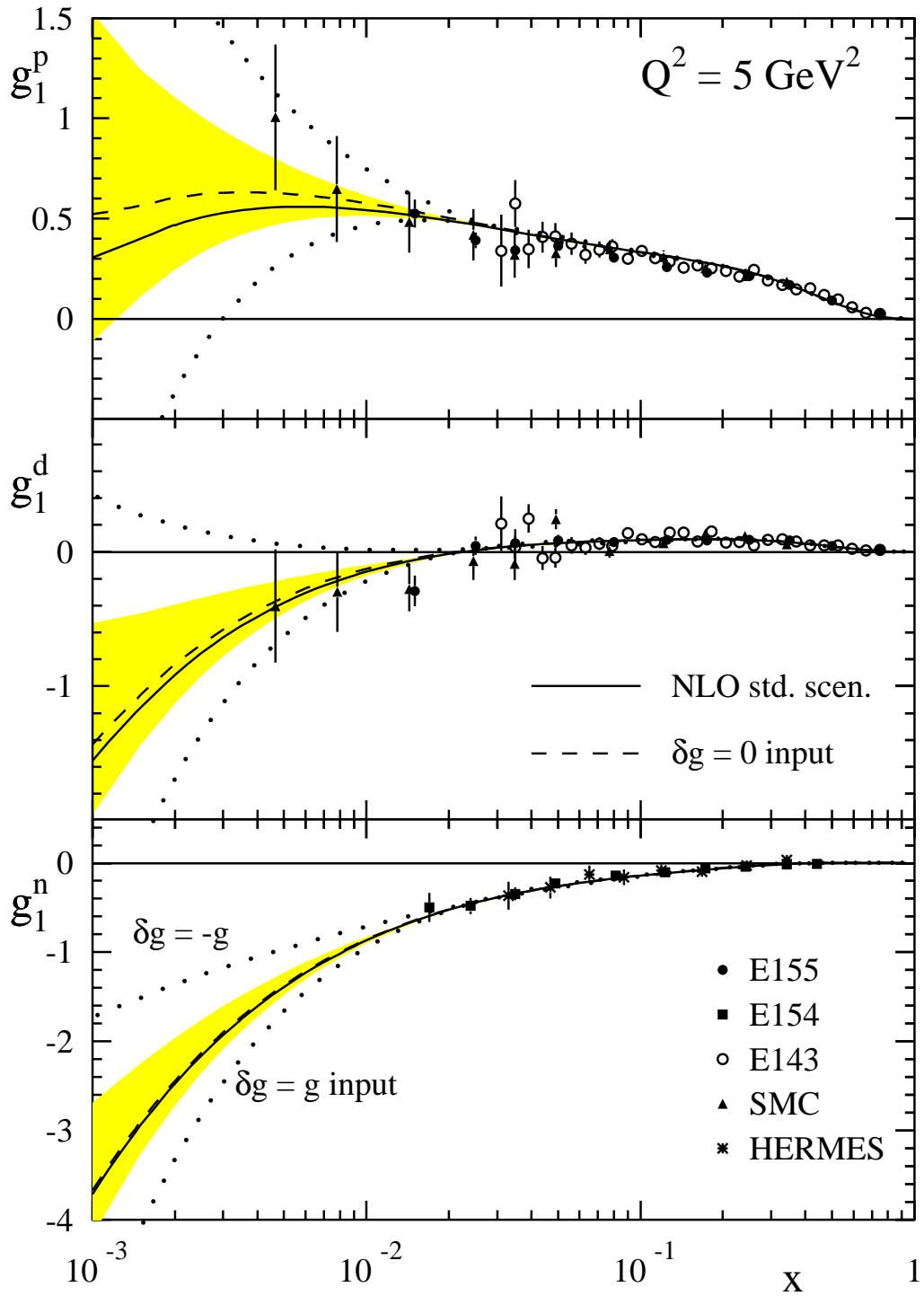


Fig. 3

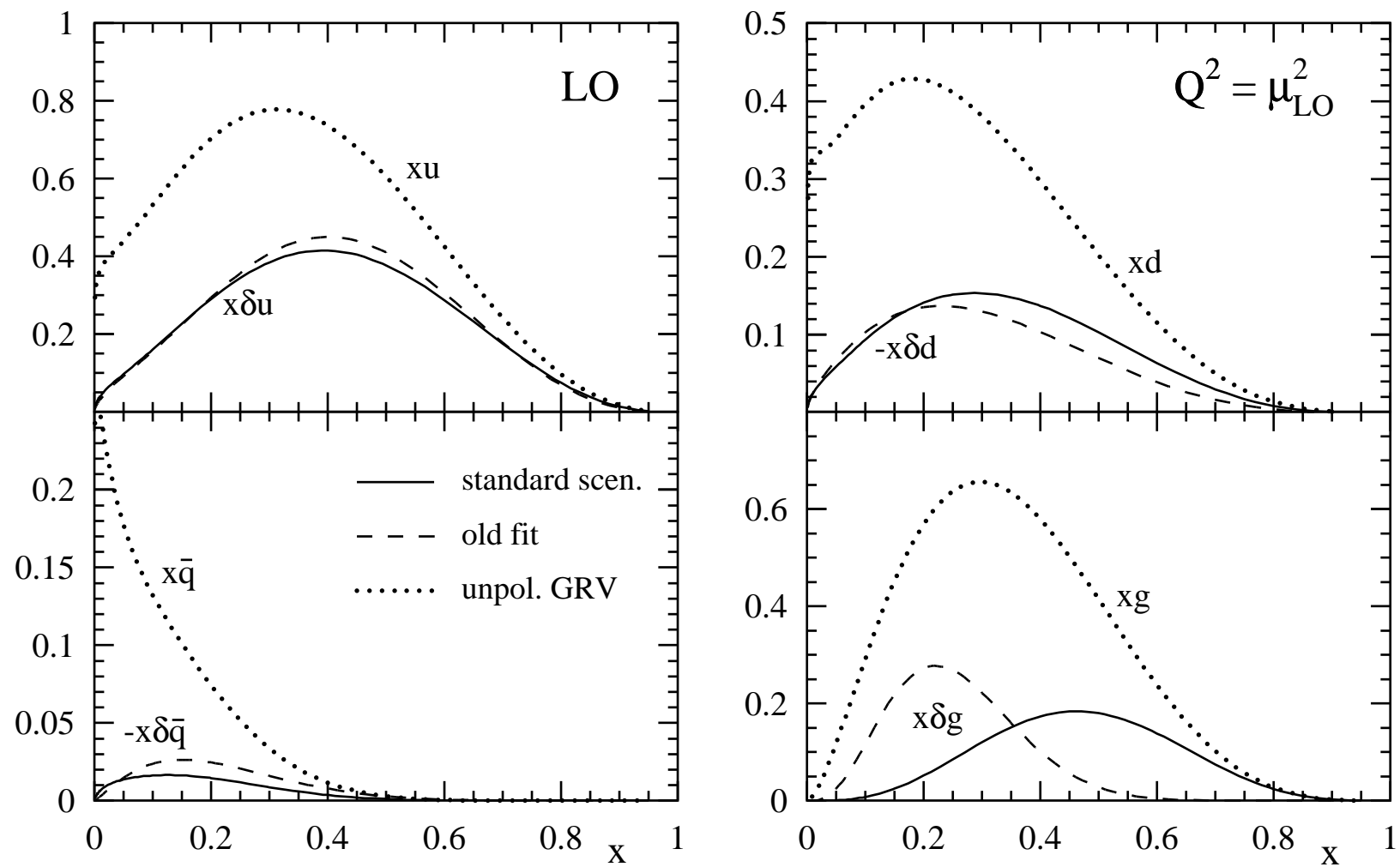


Fig. 4(a)

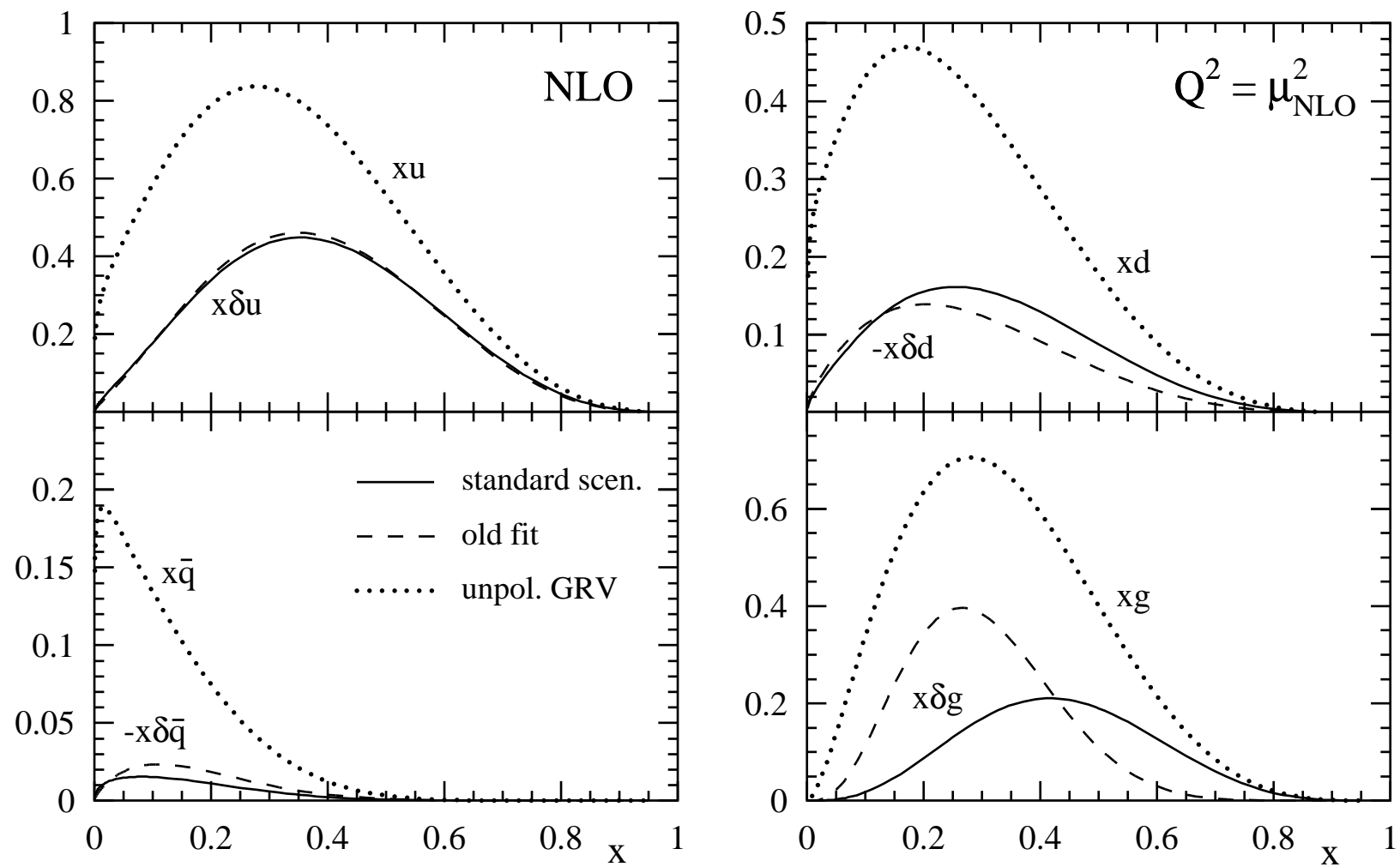


Fig. 4(b)



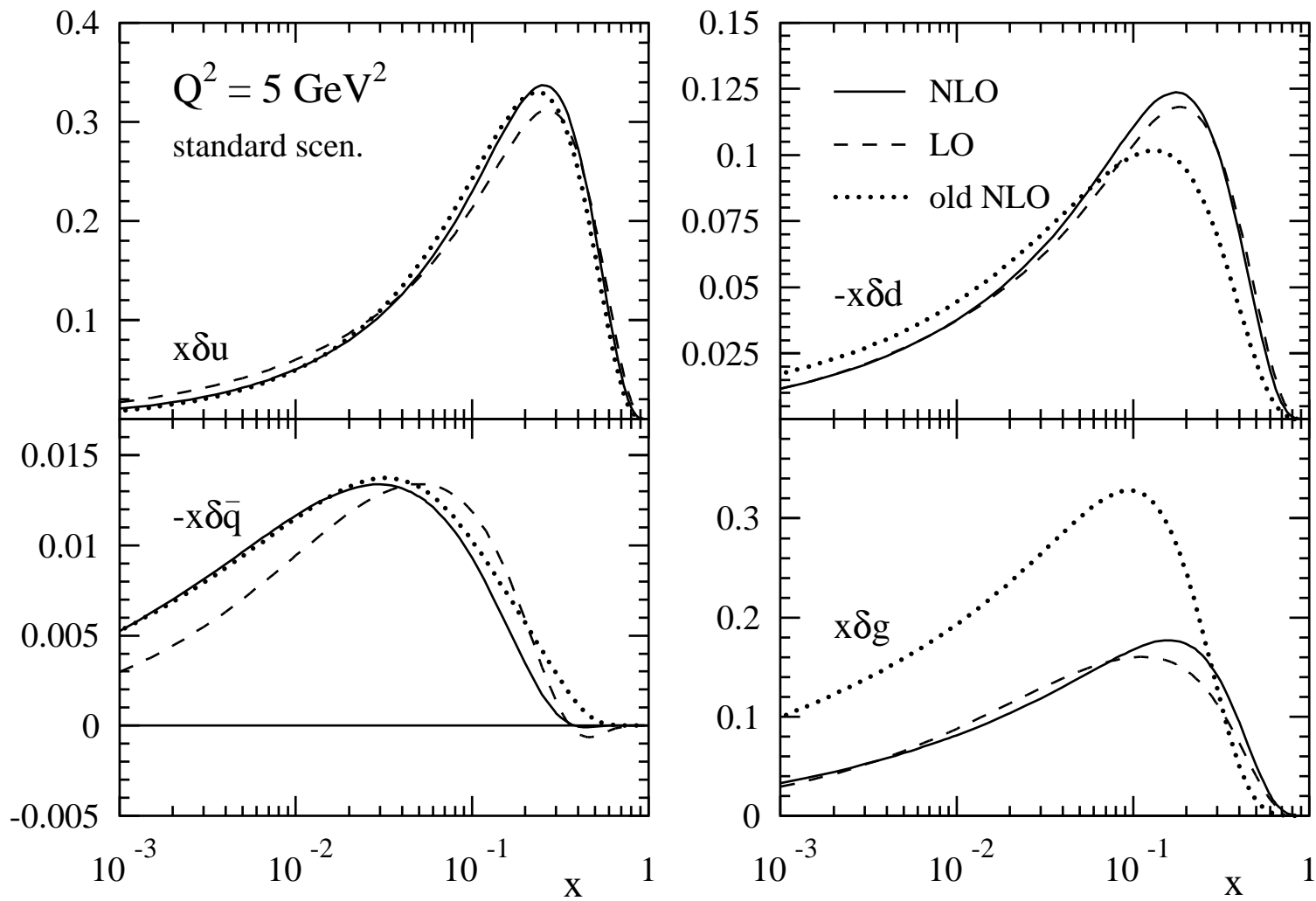


Fig. 5

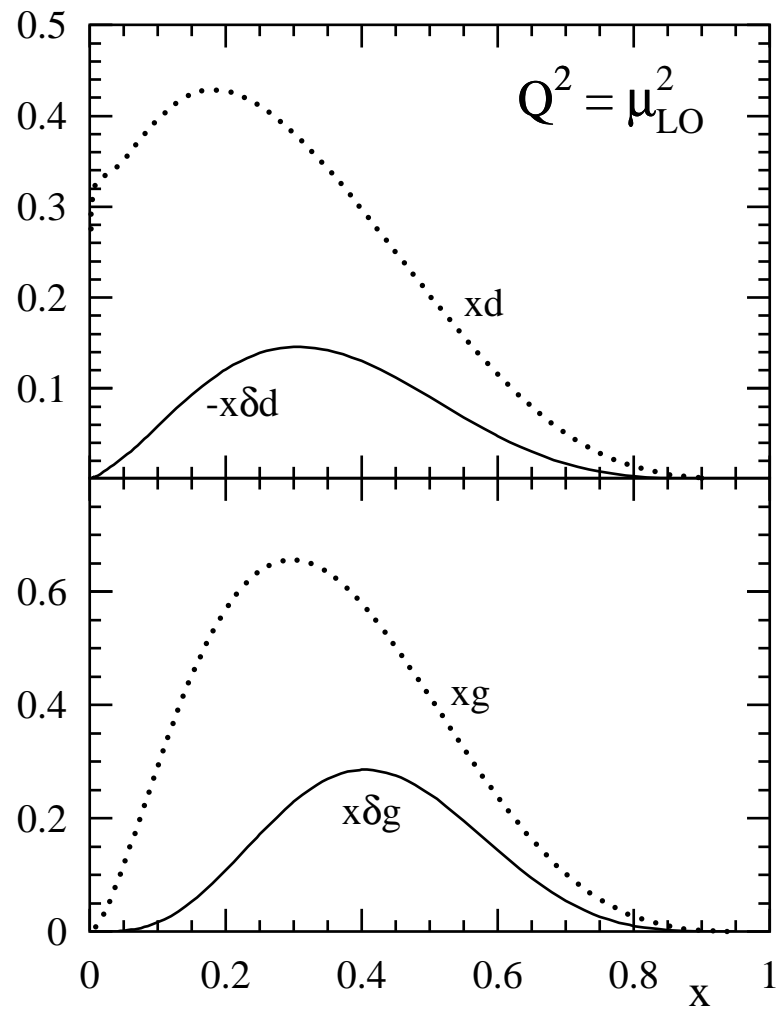
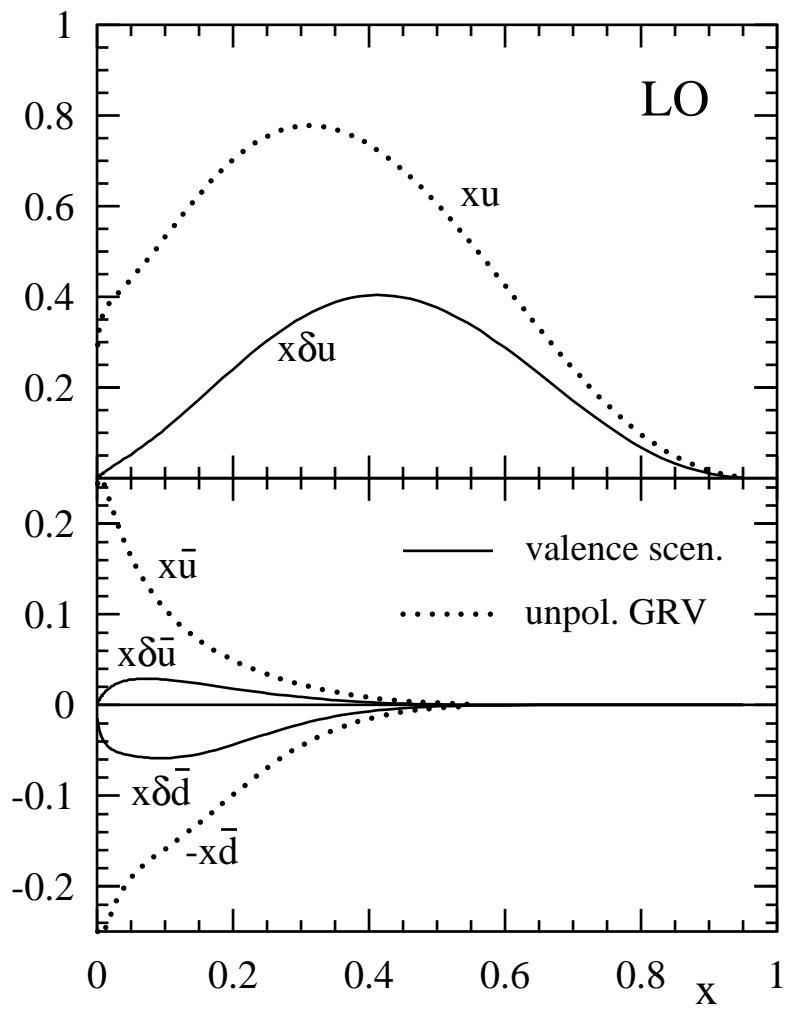


Fig. 6(a)

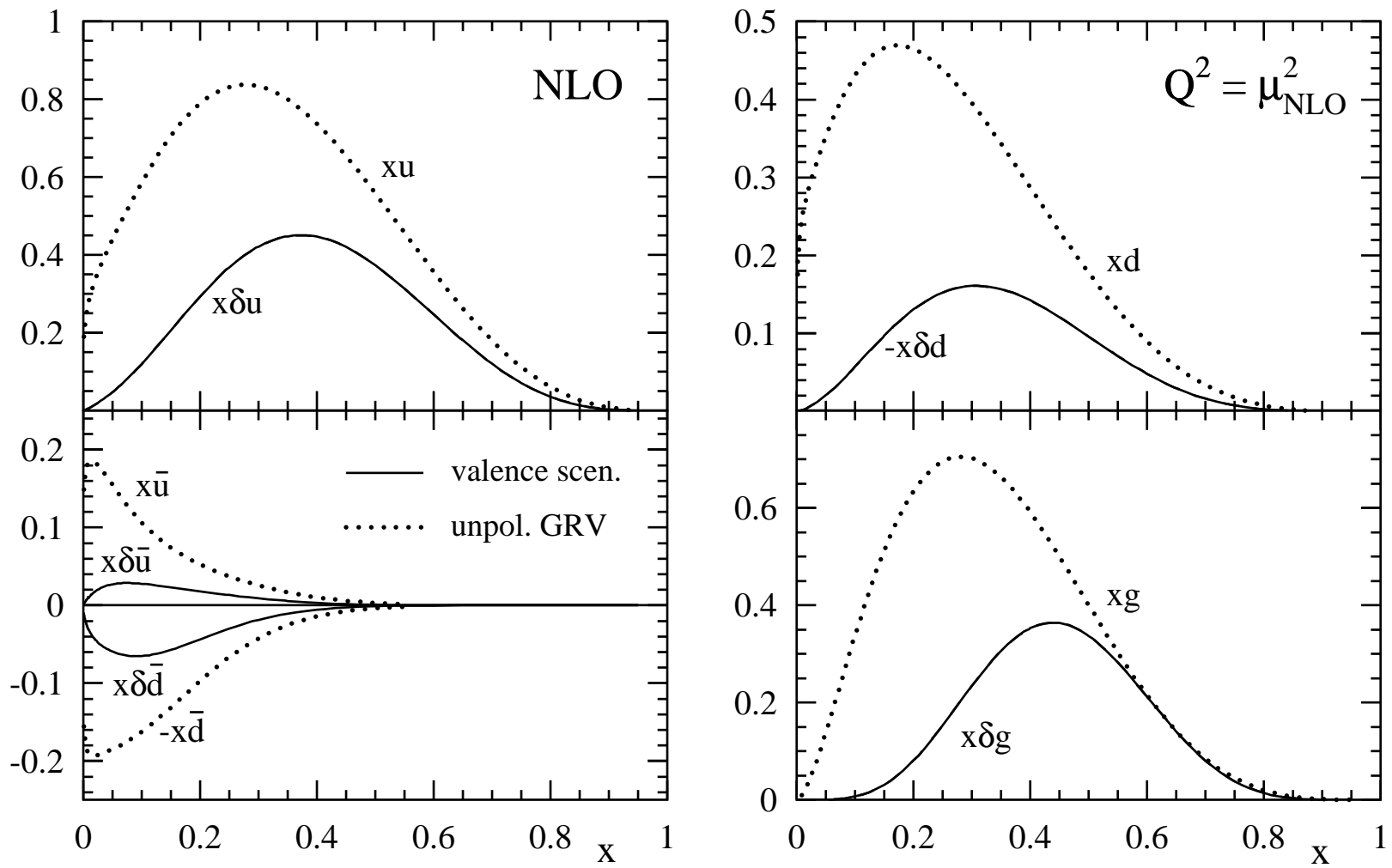


Fig. 6(b)

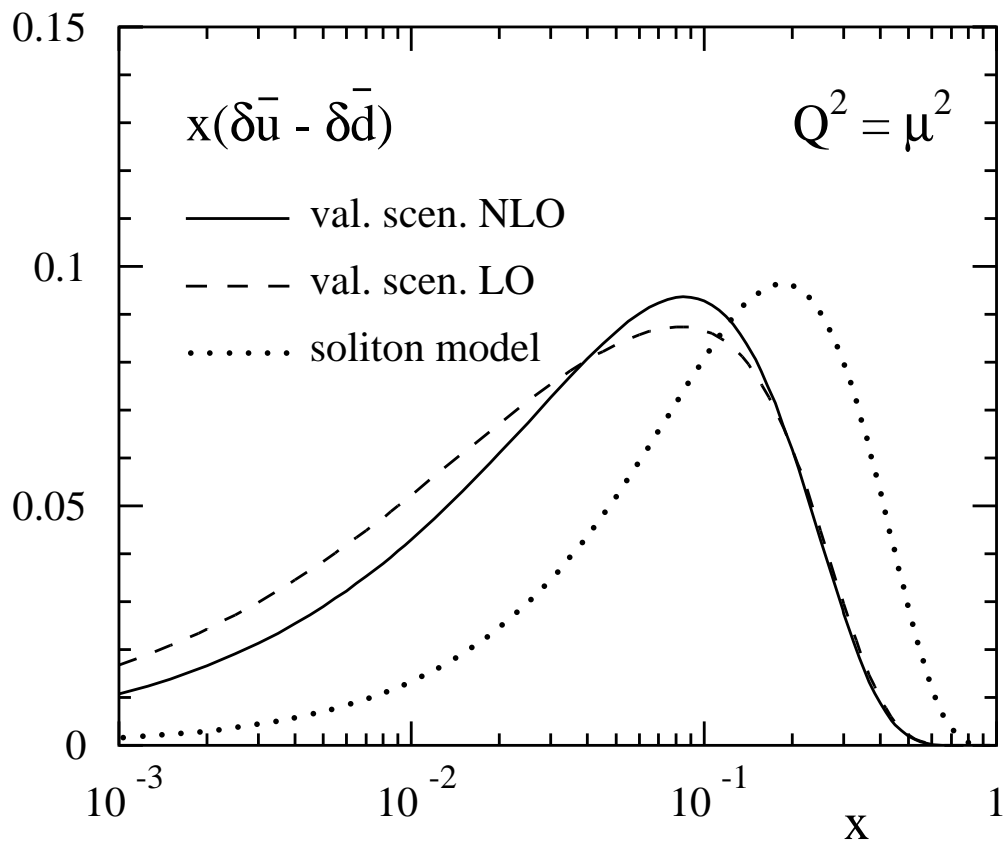


Fig. 7

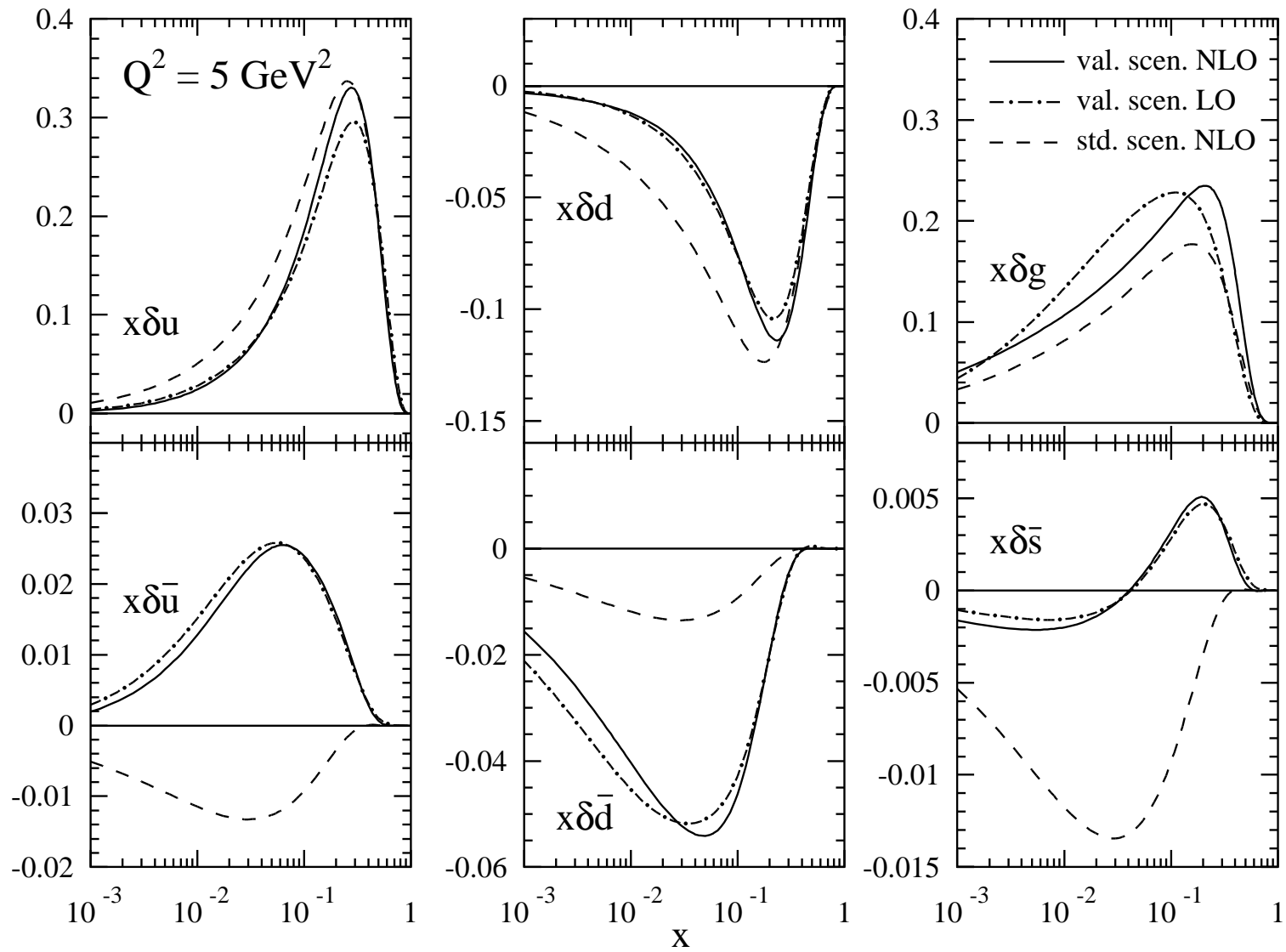


Fig. 8

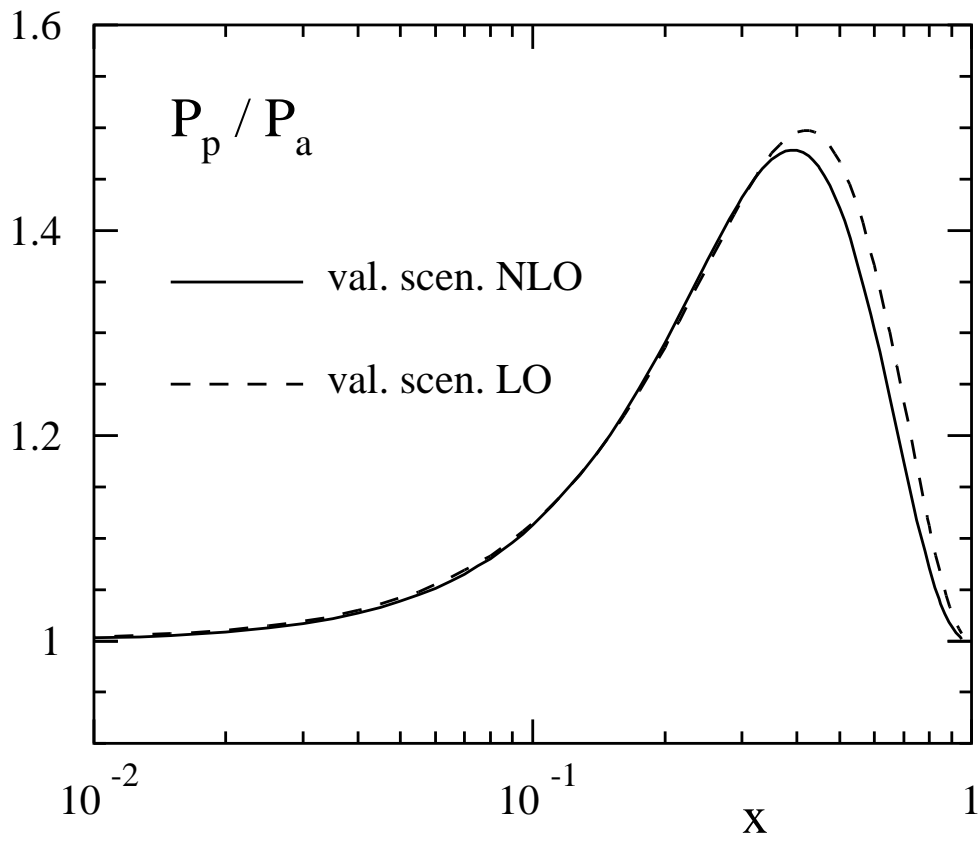


Fig. 9

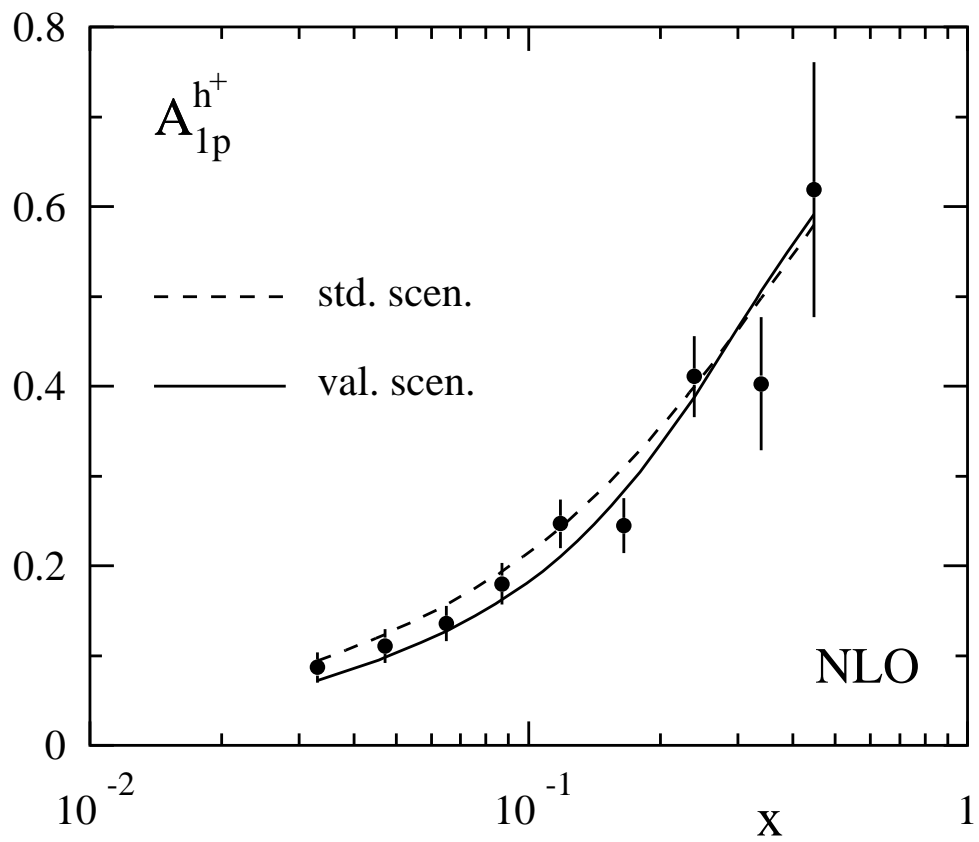


Fig. 10